Pseudo-first-order reaction of chemically and biologically formed green rusts with HgII and C15H15N3O2: effects of pH and stabilizing agents (phosphate, silicate, polyacrylic acid, and bacterial cells)

P-Ph Remy, M. Etique, A. A. Hazotte, A-S Sergent, N. Estrade, C. Cloquet, K. Hanna, F. P. A. Jorand

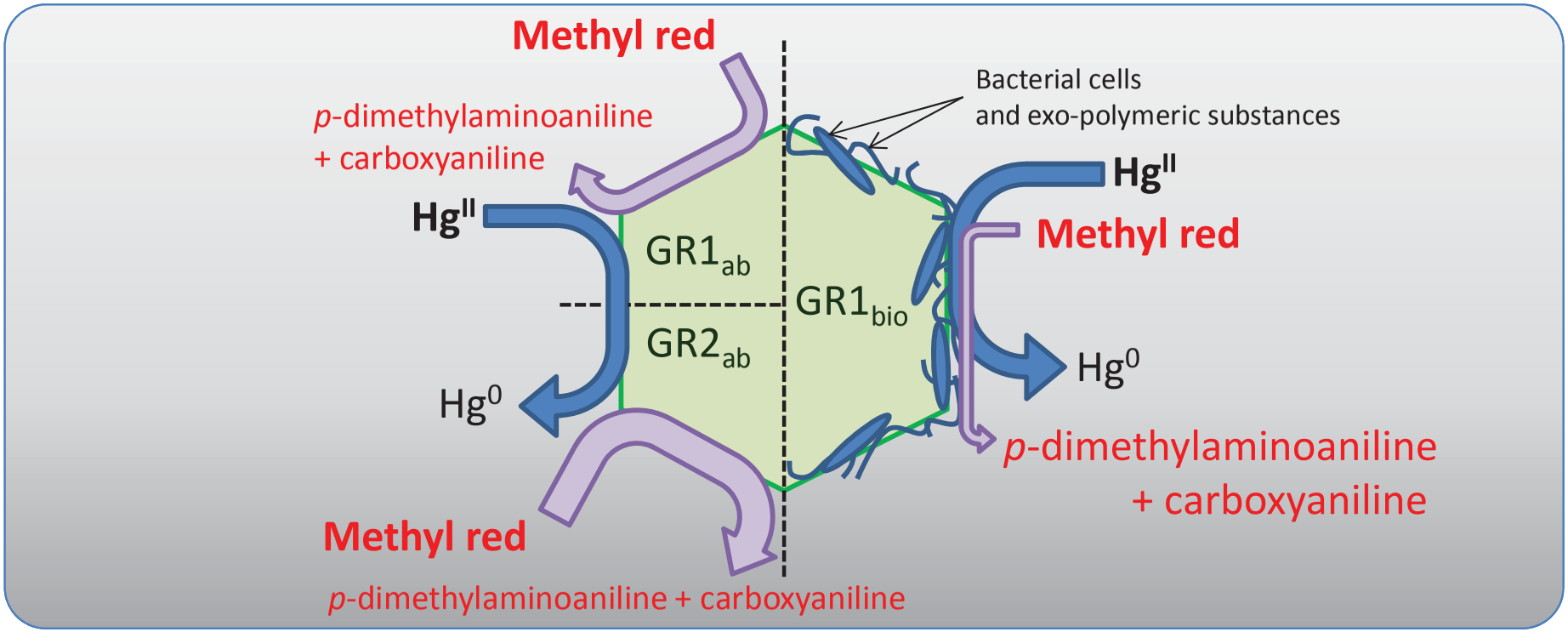
Methyl red
p-dimethylaminoaniline
+ carboxyaniline
Hg^II
GR1ab
GR2ab
Hg^0
Methyl red
p-dimethylaminoaniline + carboxyaniline
Bacterial cells
and exo-polymeric substances
GR1bio
Hg^II
Methyl red
Hg^0
p-dimethylaminoaniline
+ carboxyaniline

Pseudo-first-order reaction of chemically and biologically formed green rusts with Hg^{II} and $C_{15}H_{15}N_3O_2$: effects of pH and stabilizing agents (phosphate, silicate, polyacrylic acid, and bacterial cells)

P.-Ph. Remy[1, 2], M. Etique[1, 2], A.A. Hazotte[1, 2,§], A.-S. Sergent[1, 2], N. Estrade[3, 4#], C. Cloquet[3, 4], K. Hanna[5, 6], and F.P.A. Jorand[1,2*]

[1]Université de Lorraine, LCPME, UMR 7564, Institut Jean Barriol, Villers-lès-Nancy, F-54601, France

[2]CNRS, LCPME, UMR 7564, Institut Jean Barriol, Villers-lès-Nancy, F-54601, France

[3]CNRS, CRPG, UMR 7358, BP 20, Vandœuvre-lès-Nancy, F-54501, France

[4]Université de Lorraine, CRPG, UMR 7358, BP 20, Vandœuvre-lès-Nancy, F-54501, France

[5]ENSCR, CNRS, UMR 6226, CS 50837, Rennes Cedex 7, F-35708, France

[6]Université européenne de Bretagne, Rennes, F-35000, France

[§]Present address: LUNAM University, Subatech-LPGN, UMR 6457 & 6112, BP 92208, F-44322 Nantes Cedex 3, France

#Present address: Pacific Centre for Isotopic and Geochemical Research, EOAS, The University of British Columbia, 2207 Main Mall, Vancouver, British Columbia, V6T 1Z4, Canada.

*Corresponding author: frederic.jorand@univ-lorraine.fr; +33 (0)383 685 248

Keywords: Reductive transformation, layered double hydroxides, cationic mercury, methyl red, biogenic green rust, surface area concentration

Abstract

The kinetics of Hg^{II} and methyl red (MR) reduction by hydroxycarbonate green rust (GR1) and by hydroxysulfate green rust (GR2) were studied in the presence of naturally occurring organic and inorganic ligands (phosphate, polyacrylic acid, bacterial cells, silicate). The reducing ability of biogenic hydroxycarbonate green rust ($GR1_{bio}$), obtained after microbial reduction of lepidocrocite by *Shewanella putrefaciens*, was also investigated and compared to those of chemically synthesized GR1 and GR2 ($GR1_{ab}$ and $GR2_{ab}$). Pseudo first-order rate constants (k_{obs}) of Hg^{II} reduction (at pH 7, 8.2, and 9.5) and MR reduction (at pH 7) were determined and were normalized to the structural Fe^{II} content of GRs (k_{FeII}) and to the estimated concentration of surface Fe^{II} sites (k_S). The k_S values ranged from 0.3 L $mmol^{-1}$ min^{-1} to 43 L $mmol^{-1}$ min^{-1} for the Hg reduction, and from 0.007 L $mmol^{-1}$ min^{-1} to 3.4 L $mmol^{-1}$ min^{-1} for the MR reduction. No significant discrepancy between GR_{ab} and GR_{bio} was observed in term of reactivity. However, the reduction kinetics of MR was generally slower than the Hg^{II} reduction kinetics for all tested GRs. While a slight difference in Hg^{II} reduction rate was noted whatever the pH values (7.0, 8.2, or 9.5), the reduction of MR was significantly affected in the presence of ligands. A decrease by a factor of 2 – 200, depending on the type of ligand used, was observed. These data give new insights into the reactivity of GRs in the presence of co-occurring organic and inorganic ligands, and have major implications in the characterization of contaminated systems as well as water treatment processes.

1. Introduction

Green rusts (GRs) are mixed ferrous–ferric hydroxides which have a layered structure characterized by alternating positively charged hydroxide layers $\{Fe^{II}_{(1-x)}Fe^{III}_{x}(OH)_2\}^{x+}$ and hydrated anionic interlayers $\{(x/n)A^{n-}\bullet mH_2O\}^{x-}$. Two types of GRs are distinguished: green rust 1 (GR1) and green rust 2 (GR2) containing either planar or spherical anions (*e.g.* CO_3^{2-}, Cl^-), and non-planar anions (*e.g.* SeO_4^{2-}, SO_4^{2-}), respectively (Génin *et al.*, 2006). GRs are present in the environment as corrosion products of Fe-based materials (Refait *et al.*, 2003), and as minerals (*e.g.* fougèrite) in hydromorphic soils (Génin *et al.*, 1998), in ground water (Christiansen *et al.*, 2009), or in suspended matter of stratified lakes (Zegeye *et al.*, 2012). GRs are described as highly reactive compounds, especially in reducing several organic and inorganic contaminants (Myneni *et al.*, 1997; Erbs *et al.*, 1999; Loyaux-Lawniczak *et al.*, 2000; Hansen *et al.*, 2001; Williams and Scherer, 2001; Lee and Batchelor, 2002; O'Loughlin *et al.*, 2003; Elsner *et al.*, 2004; O'Loughlin *et al.*, 2004; Mitsunobu *et al.*, 2008; Kone *et al.*, 2009) and their roles in the biogeochemical redox cycling of iron and other elements are of growing interest to the scientific community (e.g. : Carlson *et al.*, 2012; Zegeye *et al.*, 2012). Although their reactivity has been widely investigated with chemically synthesized GR2 (SO_4^{2-}), the reactivity of GR1, microbially synthesized GR1/GR2, and GR2 in the presence of cells or polymers has been scarcely reported.

GRs can be synthesized at the laboratory scale by a partial oxidation of ferrous salts or by a coprecipitation of Fe^{II} with Fe^{III} salts in aqueous solution (Schwertmann and Fechter, 1994; Génin *et al.*, 1998; Bocher *et al.*, 2004). They can also be formed by bacterial activities via a bioreduction of ferrihydrite or lepidocrocite under anoxic conditions (Fredrickson *et al.*, 1998; Ona-Nguema *et al.*, 2002) or by an indirect Fe^{II} oxidation by biogenic nitrite (Etique *et al.*, 2014a). In the natural environment, the formation of GRs is sometimes incorrectly considered as a biological process, whereas the reduction of Fe^{III} species or the oxidation of

Fe^{II} species are only due to an enzymatic reaction. The resulting coprecipitation leading to the formation of GR in the extracellular medium is only based on a chemical process. Furthermore, no difference in structure and composition between chemically and biologically formed GRs have been evidenced, except for the size of crystals, which are larger for the biological GR than for its chemical counterpart (Zegeye *et al.*, 2005), and for the presence of extracellular-polymeric substances (EPS) and/or bacterial cells surrounding biological GR crystals (Zegeye *et al.*, 2010; Jorand *et al.*, 2013). These EPS and cells are perceived as affecting GR reactivity, which might explain the higher stability of the biogenic GR (for several years in aqueous phase) as compared to the chemical one. However, this phenomenon remains poorly studied and barely understood. Although recent work has demonstrated that the extracellular polymers (EPS from activated sludge in waste water treatment) significantly affect the reactivity of GR1 towards anionic inorganic pollutants (NO_3^-), probably by "screen effect" on reactive sites (Zegeye *et al.*, 2014), knowledge on this reactivity with metallic or organic contaminants is essential to provide greater insight into applied or natural processes in which GRs are involved (*e.g.* Su and Puls, 2004; Bearcock *et al.*, 2011).

For that purpose, the reactivity of a biologically/chemically synthesized hydroxycarbonate GR1 ($GR1_{bio}$/$GR1_{ab}$), and chemically formed sulfate GR2 ($GR2_{ab}$) towards Hg^{II} and $C_{15}H_{15}N_3O_2$ (methyl red MR) was investigated in presence of various stabilizing agents. Previous works have already studied the reactivity of $GR2_{ab}$ towards Hg^{II} and MR (O'Loughlin *et al.*, 2003; Kone *et al.*, 2009), but to the best of our knowledge, the reactivity of biogenic GRs towards these two contaminants has not yet been documented. In anoxic environments, green rust phases are represented by the fougèrite mineral, which is a hydroxycarbonate green rust (GR1) (Génin *et al.*, 1998; Mills *et al.*, 2012). Therefore, the most representative iron phase of this fougérite mineral would be the $GR1_{bio}$. $GR2_{ab}$ is known to be relatively stable as long as common anoxic conditions are preserved at pH ~7 (Ruby *et*

al., 2006), while $GR1_{ab}$ is perceived as unstable iron hydroxides rapidly turning into a mixture of magnetite ($Fe^{II}Fe^{III}_2O_4$) and siderite ($FeCO_3$) (Taylor *et al.*, 1985; Benali *et al.*, 2001). However, under strict anoxic conditions and neutral to slightly alkaline pH (7 – 9) (this work), $GR1_{ab}$ can be preserved and stored for several days (Etique *et al.*, 2014b). Nonetheless, many experiments were performed with $GR1_{ab}$ supplemented with PO_4^{3-} that prevents any further undesirable "transformation" (Bocher *et al.*, 2004). Silicate, quartz, organic polymers, and bacterial cells – compounds which are commonly found in environmental settings or in water or soil remediation processes – were also described to inhibit/prevent GRs dissolution/transformation (Zegeye *et al.*, 2010; O'Loughlin *et al.*, 2010; Sergent *et al.*, 2011; Jorand *et al.*, 2013). Thus, to test the ability of these "stabilizers" to affect the reactivity of GR1 and GR2, the reduction of Hg^{II} and MR was carried out in the presence of phosphates, silicates, polyacrylic acid (paa), and bacterial cells, at pH values allowing a stability of GRs (pH > 7). Control experiments were also performed to evaluate the contribution of aqueous Fe^{II} and bacterial cells to the transformation of target compounds. The depletion of mercury was monitored over time using ICP-AAS. The MR reduction was monitored by UV-Visible spectrophotometry.

2. Chemical background

2.1. Mercury and GR

Mercury has two main stable oxidation states: Hg^0 and Hg^{II}. Elemental Hg^0 is gaseous under environmental conditions, and under environmentally relevant pH values Hg^{II} exists in pure water in aqueous form as Hg^{2+} and mercury dihydroxide ($Hg(OH)_2$) (1) with a p*Ka* value of 6.09 (Pourbaix, 1963):

$$Hg^{2+} + 2OH^- = Hg(OH)_2 \quad (1)$$

Thus, the predominant mercury species with pH higher than or equal to 6.09 is $Hg(OH)_2$, and the reduction half-reaction equation (2) is:

$$Hg(OH)_2 + 2H^+ + 2e^- = Hg^0 + 2H_2O \qquad E° = 1.034\ V \qquad (2)$$

The reduction of Hg^{II} is effective in the presence of solid Fe^{II} but insignificant with aqueous Fe^{II} (Charlet *et al.*, 2002). The mixed Fe^{II}-Fe^{III} minerals, such as sulfate GR2, are oxidized by Hg^{II} to magnetite (O'Loughlin *et al.* 2003). The Fe^{II}/Fe^{III} ratio of hydroxycarbonate GR1 can vary from 1/2 to 2/1 (trébeurdenite and fougèrite, respectively) (Mills *et al.*, 2012), while it is equal to 2/1 for sulfate GR2, as far as we know (Refait *et al.*, 2006). The oxidation of GR1 and GR2 to magnetite by $Hg(OH)_2$ involves an exchange of 2 electrons and is given by equations (3) and (4):

$$Fe^{II}_4Fe^{III}_2(OH)_{12}CO_3 + Hg(OH)_2 = 2Fe_3O_4 + Hg^0 + HCO_3^{2-} + 6H_2O + H^+ \qquad (3)$$

$$Fe^{II}_4Fe^{III}_2(OH)_{12}SO_4 + Hg(OH)_2 = 2Fe_3O_4 + Hg^0 + SO_4^{2-} + 6H_2O + 2H^+ \qquad (4)$$

Due to the presence of bicarbonate, the oxidation of GR1 leads to a lower production of H^+ than that of GR2.

2.2. Methyl red and GR

Methyl red (MR) or 2-(N,N-dimethyl-4-aminophenyl)azobenzenecarboxylic acid ($C_{15}H_{15}N_3O_2$) is an azo dye with one azo group (-N=N-) used as a common pH indicator with a *pKa* = 5.1. As other azo dyes, MR is a recalcitrant pollutant causing a significant burden on the environment. The reduction of MR is known to be achieved with the cleavage of the azo bond (Khalid *et al.*, 2008; Kone *et al.*, 2009), leading to the formation of two aromatic amines (carboxyanilic acid: R_1-NH_2 and *p*-dimethylaminoaniline: R_2-NH_2) as:

$$R_1\text{-}N{=}N\text{-}R_2 + 4H^+ = R_1\text{-}NH_2 + R_2\text{-}NH_2 + 4e^- \qquad (5)$$

Thus, 4 Fe^{II}_{GR} are theoretically needed to reduce MR and, assuming that GR is oxidized into FeOOH, the reduction equations can be written as:

$$Fe^{II}_4Fe^{III}_2(OH)_{12}CO_3 + R_1\text{-}N{=}N\text{-}R_2 = 6FeOOH + HCO_3^{2-} + R_1\text{-}NH_2 + R_2\text{-}NH_2 + H^+ \qquad (6)$$

144 $Fe^{II}_4Fe^{III}_2(OH)_{12}SO_4 + R_1\text{-}N{=}N\text{-}R_2 = 6FeOOH + SO_4^{2-} + R_1\text{-}NH_2 + R_2\text{-}NH_2 + 2H^+$ (7)

145

146 # 3. Materials and methods

147

148 ## 3.1. Chemicals

149 All solutions were prepared using ACS grade chemicals (except when specified) and 18.2
150 MΩ cm N_2-purged pure water (Purelab Option-Q, Elga LabWater, Antony, France). The
151 mercury solution (750 µM) was prepared from an $HgCl_2$ salt 99.5% (1166745, Merck) in HCl
152 0.5 M (30721-2.5L, Sigma-Aldrich) and the pH was adjusted to 7.0 ± 0.1 with NaOH 1M.
153 Ferrous sulfate heptahydrate ($FeSO_4•7H_2O$, 99%), ferrous chloride tetrahydrate ($FeCl_2•4H_2O$,
154 99%), and sodium phosphate ($Na_2HPO_4•7H_2O$) were purchased from Sigma-Aldrich.
155 Polyacrylic acid $(C_3H_4O_2)_n$ was provided from a stock solution of 2 g L^{-1} (Mw 2,000 g mol^{-1},
156 Aldrich, 323667). The methyl red ($C_{15}H_{15}N_3O_2$) was provided by Sigma-Aldrich (98%,
157 32654-25G).
158 The mercury concentration present in each reactant (0.3 – 1.9 ppb) was measured as blank
159 (Table S1).

160

161 ## 3.2. Synthesis of GRs

162 Abiotically formed GRs were synthesized under O_2-free conditions in an anaerobic
163 chamber scavenging oxygen with palladium catalysts and H_2 (N_2/H_2, 95/5) (Coy Laboratory
164 Products Inc.®). The $GR1_{ab}$ was obtained using a coprecipitation method as described by
165 Bocher *et al.* (2004) by adding a mixture of Fe^{II} and Fe^{III} salts to a mixture of sodium
166 hydroxide and sodium carbonate. Ferrous sulfate heptahydrate $FeSO_4•7H_2O$ and ferric sulfate
167 pentahydrate $Fe_2(SO_4)_3•5H_2O$ were dissolved in 40 mL of pure water. A $[Fe^{II}]/[Fe^{III}]$ ratio of
168 2 was chosen with $\{[Fe^{II}]+[Fe^{III}]\} = 0.5$ M. Magnetic stirring (500 rpm) ensured fast and

complete dissolution. Di-sodium carbonate Na_2CO_3 ($[CO_3^{2-}]$ = 0.5 M) was dissolved in 40 mL of a 1 M NaOH solution in order to have $[OH^-]/\{[Fe^{II}]+[Fe^{III}]\}$ = 2. The carbonate solution was added to the solution of iron under the same conditions of magnetic stirring, and a bluish-green precipitate appeared immediately. $GR1_{ab}$ was used within a week of its formation to test its reactivity with Hg^{II} and MR, or was stabilized by addition of extra $Na_2HPO_4•7H_2O$ salt $\{[PO_4]_0/[Fe]\}$ = 0.8% (*i.e.* 4 mM PO_4^{3-}) ($GR1_{ab+P}$) or silicic acid (H_4SiO_4 4 mM) ($GR1_{ab+Si}$), or paa (500 mg L^{-1}) ($GR1_{ab+paa}$). A $\{[CO_3^{2-}]/[SO_4^{2-}]\}$ ratio of 1 was chosen to prevent the formation of sulfate $GR2_{ab}$ as described by Bocher *et al.* (2004).

The abiotic sulfate GR2 ($GR2_{ab}$) was synthesized using the coprecipitation method developed by Ruby *et al.* (2003). Briefly, 20 millimoles of an iron solution, containing 13.3 millimoles Fe^{II} (3.7 g of $FeSO_4•7H2O$) and 6.7 millimoles Fe^{III} (1.63 g of $Fe_2(SO_4)_3•5H_2O$), were added to 400 mL of pure water. Iron salts were precipitated by addition of NaOH (50 mL, 40 mM) with a syringe and under magnetic stirring to precipitate all the iron salts (nNaOH / nFe = 2).

The biotic carbonate GR1 ($GR1_{bio}$) was produced according to Zegeye *et al.* (2007) by incubation of *S. putrefaciens* CIP 8040^T (2.5×10^9 cells mL^{-1}) at 30°C in a basal medium containing 160 mM of sodium formate (HCOONa) and 300 mM of lepidocrocite (γ-FeOOH) as the sole electron donor and acceptor, respectively.

All GRs synthesized were washed in O_2-free deionized water by centrifugation (5 min, 10,000 × *g*) and the concentration of GRs was determined by the spectrophotometric ferrozine method measuring the concentration of Fe^{II} and Fe^{total} (Viollier *et al.*, 2000) after HCl extraction (6 M) in a Tecan Infinite M200 PRO microplate reader. GRs were characterized by X-ray diffraction (XRD), transmission electron microscopy (TEM), and transmission Mössbauer spectroscopy (TMS).

3.3. Experimental set-up of Hg^{II} and methyl red reduction by GRs

The Hg^{II} solution (5 µM, initial starting concentration) was introduced into a 250 mL glass reactor (borosilicated glass, Schott) containing 150 mL of pure water with a GR suspension (500 µM, Hg/GR = 1/100). Initially, the glass reactor pH was adjusted to 7.0, 8.2, and 9.5 with NaOH 1N or HCl 0.5N. The glass reactor was continuously N_2-purged and stirred (300 rpm) in order to outgas Hg^0 and prevent any oxidation from ambient air. One milliliter of the unfiltered suspension (*i.e.* with dissolved and adsorbed Hg) was sampled at regular time intervals and was immediately dissolved in an acidic solution of HNO_3/HCl (500 µL HNO_3 at 65% with 500 µL HCl at 30%, w/v), before being diluted ten times. This acidic digestion was performed in order 1) to stop the reaction and preserve the mercury speciation, and 2) to dissolve the mineral phase and to release the potential adsorbed Hg fraction in the aqueous phase. Thus, the potential adsorption of Hg on GR surfaces should not bias the determination of reduction kinetic. Moreover, the formation of Hg^0 was qualitatively checked by trapping it during the reaction between Hg^{II} species and green rust in a solution of $KMnO_4$ 50 mM (in H_2SO_4 10%), where the elemental volatile mercury was re-oxidized into Hg^{II} under acidic conditions (data not shown).

The methyl red (MR) solution was prepared in pure water and the pH was adjusted to 7.0 ± 0.1 with NaOH 1N. The MR solution (final concentration ~15 µM) was introduced in a glass batch reactor containing 150 mL of pure water with a GR suspension (500 µM, MR/GR ~1/33). During the reaction, the medium was continuously stirred (300 rpm) and 1 mL samples were removed over time after adjusting the pH to 7.0 ± 0.1 in order to avoid shifting the maximum peak (at 430 nm).

Control experiments were also carried out for Hg^{II} and MR on the same terms as before, respectively. The Fe^{II}_{aq} control was performed (0.2 mM, pH 7) to assess the reactivity of Hg^{II} or MR with aqueous Fe^{II} *versus* structural Fe^{II}. Such amounts of Fe^{II} were chosen assuming

219 that ~0.2 mM of Fe^{II}_{aq} (*i.e.* passing through 0.2 µm) was measured in a suspension of GR (not
220 shown). A bacterial control with 6×10^5 cells mL^{-1} of *S. putrefaciens* was performed to
221 evaluate the effect of bacteria in the $GR1_{bio}$ suspension. The cell density selected was similar
222 to what is required for 500 µM $GR1_{bio}$.
223
224 **3.4. Analyses**
225 The Hg concentration was determined with a Milestone DMA-80 Direct Mercury
226 Analyzer (Milestone GmbH, Germany). Its unique processing of samples by thermal
227 decomposition, amalgamation, and atomic absorption spectrometry provides a direct analysis
228 of the sample matrices.
229 The MR concentration was measured by a spectrophotometric analytical method (Cary
230 60 UV-Vis, Agilent Technologies). A broad band in the visible MR spectrum was
231 characterized at 430 nm in pH 7 (Fig. S1) and was assigned to the azo band (Hou *et al*., 2007).
232 To avoid artifacts caused by suspended particles, short centrifugations were performed (2 min,
233 14,000 × *g*) before determining MR concentration. The sorption of MR by GR was not
234 considered here, as we assumed it to be negligible as previously shown (Kone *et al.*, 2009).
235 XRD data were collected with a D8 Bruker diffractometer, equipped with a
236 monochromator and a position-sensitive detector. The X-ray source was a Co anode (k =
237 0.17902 nm). The diffractogram was recorded in the 3-64 2θ range, with a 0.0359° step size
238 and collecting time of 3 s per point.
239 TMS analyses were performed using a constant-acceleration spectrometer with a 50
240 mCi source of ^{57}Co in Rh. The spectrometer was calibrated with a 25 µm foil of α - Fe at
241 room temperature. The cryostat consisted of a closed cycle helium Mössbauer cryogenic
242 workstation with vibration isolation stand manufactured by Advance Research Systems®.
243 Helium exchange gas was used to thermally couple the sample to the refrigerator, allowing

variable temperature operations from 7 to 300 K. Computer fittings were done using Lorentzian-shape lines.

Transmission electron microscopy was conducted using CM20/STEM Philips coupled with an energy dispersive X-ray system (EDX) using a voltage of 200 kV. One drop of the suspension was laid on an amorphous carbon-coated grid and loaded into the analysis holder of the microscope under 10^{-8} Torr vacuum.

The surface area of GRs was determined by multipoint N_2-BET analysis using a Coulter (SA113) surface area analyzer. Prior to specific surface area determination, GR suspensions were dried by vacuum desiccation for 48 h.

4. Results and discussion

4.1. Characterization of GRs

The greenish solid phase formed by either the microbial reduction of lepidocrocite (γ-FeOOH) by *S. putrefaciens* or chemical synthesis was characterized by XRD (Fig. 1a) and the d-values obtained were summarized in Table S2. The carbonate GR1 was identified as a major secondary iron mineral produced by the bacterial activity ($GR1_{bio}$) and as a main product from the coprecipitation method in the presence of carbonate and stabilized with phosphate ($GR1_{ab+P}$) or not stabilized ($GR1_{ab}$), which is in close agreement with previous studies (Drissi *et al.*, 1995; Zegeye *et al.*, 2007). TEM images and electron diffraction patterns were also performed and hexagonal crystals of GR1 were observed in various sizes from 5 µm to 10 µm for $GR1_{bio}$ and from 100 nm to 300 nm for $GR1_{ab+P}$ (Fig. 1b, c and d). This is consistent with the values reported in previous investigations (Ona-Nguema *et al.*, 2002; Zegeye *et al.*, 2014).

The formation of hydroxysulfate GR2 ($GR2_{ab}$) by the coprecipitation method from Ruby *et al.* (2003) was confirmed both by the d-values from the XRD diffractogram and by

the electron diffraction pattern, which is in agreement with the literature (Simon *et al*., 1997) (Fig. 1, Table S2). Hexagonal particles of $GR2_{ab}$ were observed by TEM with sizes ranging from 200 to 400 nm, which is in line with what Zegeye *et al.* (2005) had reported.

All the GRs formed were quasi-free of crystallographic impurities at a discernible level of XRD (Fig. S2). The Fe^{II}/Fe^{III} ratio was determined by TMS or by ferrozine method on solids (Fig. S3, Table S3): 1.2 ($GR1_{ab+P}$) ≤ 1.6 ($GR1_{bio}$) ≤ 2.0 ($GR2_{ab}$) ≤ 2.2 $GR1_{ab}$, and the specific surface area (SSA) was also measured by N_2-BET analysis (Table 1): 13 $m^2\ g^{-1}$ ($GR1_{bio}$) ≤ 14 ± 2 $m^2\ g^{-1}$ ($GR2_{ab}$) ≤ 31 ± 6 $m^2\ g^{-1}$ ($GR1_{ab+P}$ and $GR1_{ab}$) and also expressed as surface area concentration (*A*) in Table 1. These SSA values of green rusts were slightly lower than those obtained by Williams and Scherer (2001): 47 ± 7 $m^2\ g^{-1}$. This fluctuation of SSA of green rusts depends on the synthesis method, which influences the crystal size. Moreover, the delay between its synthesis and its use modifies the crystal size probably by an Ostwald ripening.

Having determined SSA for each GR, the concentration of the surface Fe^{II} sites available can be reasonably estimated since the reactivity of GRs is based on this value. Here, an example is given for $GR1_{bio}$ with an initial concentration of 500 µM and with the *A* value of 4.2 $m^2\ L^{-1}$ (Table 1). Knowing that the average common value of the surface site density is 5 Fe^{II} sites per nm^2 for iron oxides (Williams and Scherer, 2001), the number of Fe^{II} sites per nm^2 and per L of $GR1_{bio}$ was determined at 2.1×10^{19} Fe^{II} sites $nm^{-2}\ L^{-1}$(i.e. 5 Fe^{II} sites nm^{-2} × 4.2×10^{18} $nm^2\ L^{-1}$). The total concentration of Fe^{II} sites on $GR1_{bio}$ surface was therefore estimated at 34.8 µM (Table 1).

4.2. Kinetics of Hg^{II} reduction by GRs

Regardless the GR species, the Hg^{II} concentrations decreased rapidly according to an exponential decay at neutral and alkaline pH values (7.0, 8.2, and 9.5) (Fig. 2). Since GRs were present in great excess, their concentrations are assumed to have been constant

294 throughout the reaction and the decrease in Hg concentration can be described by a pseudo
295 first-order reaction (equations 8, 9):

296 $$d[Hg]_t/dt = -k_{obs} \times [Hg]_t \quad (8)$$

297 $$[Hg]_t = [Hg]_0 \times \exp(-k_{obs} \times t) \quad (9)$$

298 where k_{obs} is the pseudo first-order rate constant (min^{-1}), and $[Hg]_t$ and $[Hg]_0$, the total
299 concentrations of cationic mercury at time *t* and *0*, respectively. The fitting by a pseudo first-
300 order reaction is consistent with other studies with GR and various oxidants such as selenite,
301 CCl_4, nitrate, and Cr^{VI} (Erbs *et al.*, 1999; Hansen *et al.*, 2001; Williams and Scherer, 2001;
302 Etique *et al.*, 2014b). The values of k_{obs} were determined from equation (9) by plotting –
303 $\ln([Hg]_t/[Hg]_0)$ as a function of time *t*. To take into account the Fe^{II} content of GRs (Note S1),
304 k_{obs} values were normalized to Fe^{II} content ($k_{Fe^{II}}$, L $mmol^{-1}$ min^{-1}) (Note S2), but it does not
305 significantly affect the hierarchy as regards the kinetic rate constants (Table 1). Similarly, a
306 k_{obs} normalization to the concentration of Fe^{II} sites on the green rust surface (k_S, L $mmol^{-1}$
307 min^{-1}) (Note S3) does not seem to influence significantly the decrease of the Hg reduction rate
308 from pH 7.0 to pH 9.5 (Table 1). However, at pH 8.2 the k_S values clearly highlight the
309 increase of Hg reduction kinetics when Hg^{II}/GR ratio increases from 1/80 to 1/0.8 for $GR1_{bio}$
310 and from 1/100 to 1/10 for $GR1_{ab}$ (Table 1, Fig. S4). Thus, this approach with k_S appeared to
311 be more relevant compared to the expressions of kinetics rate constants in k_{obs} and k_{FeII}.

312 Control tests were performed with aqueous Fe^{II} (0.2 mM, pH = 7.0) or with bacteria (pH
313 = 7.0) and no significant decrease in Hg concentration was observed over time ($k_{obs} < 10^{-3}$
314 min^{-1}) (Fig. S5a). This indicates that the depletion of Hg is neither due to a reduction reaction
315 with the aqueous Fe^{II}, nor to sorption on glass walls. Similarly, bacteria associated with
316 $GR1_{bio}$ do not appear to be responsible for the Hg^{II} decrease. Thus, *S. putrefaciens* is not able,
317 in our experimental conditions, to reduce Hg^{II}. It is worth noting that other iron reducers such
318 as *S. oneidensis* MR-1 or *Geobacter* spp are able to reduce Hg^{2+} especially with lower

amounts of Hg^{II} (0.15 µM) and under growth conditions (Wiatrowski *et al.* 2006). In the present work, *S. putrefaciens* was in stationary growth phase and no electron donor or carbon source were added (non-growth conditions).

These results demonstrate that GRs reduced effectively Hg^{II} to Hg^{0}. Compared to other Fe^{II} solids, these reaction kinetics are of the same order of magnitude as those induced by magnetite (Wiatroswky *et al.*, 2006) or by the Fe^{II} species sorbed onto phlogopite (Charlet *et al.*, 2002). O'Loughlin *et al.* (2003) have reported slightly higher rates of Hg^{II} reduction by GR2, as they reduced 98.7% of the initial Hg^{II} (6.4 mmol L^{-1} of $GR2_{ab}$ with 400 µmol L^{-1} Hg^{II}, GR/Hg^{II} = 16) after 30 min. Here, we report a thorough reduction of Hg^{II} in less than an hour (with a ratio 6 times higher GR/Hg^{II} = 100 as compared to O'Loughlin *et al.*, 2003). Nevertheless, it cannot be excluded that part of Hg^{0} could still be trapped in the solid phase, which would underestimate the kinetics of Hg^{II} reduction (Pasakarnis *et al.*, 2013).

4.2.1. Evolution of the Fe^{II} concentration and determination of the stoichiometry of the reduction of Hg^{II} species by GRs

The green rust reactivity was also evaluated by measuring the evolution of the total Fe^{II} concentration of the suspension. Among all experiments, only 3 runs present a detectable decrease of the Fe^{II}/Fe_{tot} ratio in the presence of Hg^{II} species for a ratio Hg^{II}/GR of 1/10 ($GR1_{ab}$) (Fig. S4a), 1/8 and 1/0.8 ($GR1_{bio}$) (Fig. S4b). For all the other experiments, the Fe^{II} concentration did not vary significantly since GR was used in large excess in comparison to the initial amount of Hg^{II} species (5 µM). During the reduction of mercury, the Fe^{II}/Fe_{tot} ratio lowered of 0.06 units for $GR1_{ab}$ (1/10) and $GR1_{bio}$ (1/8) (Fig. S4). However, a sharp decrease from 0.67 to 0.46 was noted for the 1/0.8 ratio of $Hg^{II}/GR1_{bio}$ (Fig. S4b). Thus, Fe^{II} species of GR were oxidized to Fe^{III} species during the reduction of Hg^{II} species, and this chemical observation was confirmed by the characterization of magnetite as end product (Fig. S6).

343 Moreover, the stoichiometry of the reaction between Fe^{II} species and Hg^{II} species was
344 determined at 1/10, 1/8 and 1/0.8 ratios of Hg^{II}/GR (Fig. 3). The expected ratio Hg^{II}:Fe^{II}_{GR}
345 corresponding to the amount of consumed Hg^{II} ions over the amount of oxidized Fe^{II} species
346 during the reduction of mercury by green rust is 1:2 according to the equation (3). This
347 theoretical ratio of Hg^{II}:Fe^{II}_{GR} was confirmed by the determination of the 1:1.9 experimental
348 ratio (Fig. 3). Thus, this is in agreement (95 %) with the stoichiometry of the reaction
349 involving the oxidation of 2 moles of ferrous iron per 1 mole of Hg^{II} reduced species.

350 **4.2.2. Effect of pH on GR reactivity**

351 In aqueous systems, GR particles act as Lewis acid and coordinate water or hydroxyl
352 groups. This is why the particles surface chemistry is highly dependent of pH value. Recently,
353 the point of zero charge (pzc) of GRs (GR1 and GR2) has been accurately determined at
354 8.3 ± 0.1 (Guilbaud *et al.*, 2013). Therefore, at pH < 8.3, the surface of GR particles is
355 protonated, leading to a positive surface charge (Fig. 4); at pH > 8.3, the GR surface is
356 negatively charged (Fig. 4). The evolution of the net surface charge of GR with pH may affect
357 the rate and the extent of the reduction of contaminants such as chromate or mercury.
358 Williams and Scherer (2001) demonstrated that the reduction of anionic pollutants such as
359 CrO_4^{2-} was enhanced by a sorption onto positively charged surface of GR. Thus, the most
360 significant reduction of Hg^{II} should be expected for a negatively charged surface of GRs (pH
361 > 8.3), where the electrostatic interactions are more favorable for Hg^{2+} sorption.

362 However, the predominant phase of mercury at pH of this study is $Hg(OH)_2$ (Fig. 4). At
363 all tested pH values and whatever GRs used ($GR2_{ab}$, $GR1_{bio}$, and $GR1_{ab+P}$), the highest value
364 of k_{obs} ($\sim 4\times10^{-2}$ min^{-1}) was obtained at pH 7.0, when GRs have a positive surface charge (Fig.
365 2a, Table 1). This would suggest, as it was previously considered for the reaction of magnetite
366 with Hg^{II} (Wiatrowsky *et al.*, 2009), that hydroxyl groups of $Hg(OH)_2$ could react with
367 protonated GR particles, thus enhancing the sorption of mercury at the surface of GR

368 followed by a reduction into Hg^0. Indeed, when pH values rise from 7.0 to 8.2 (or 9.5), the
369 values of k_{obs} for $GR1_{ab+P}$, $GR1_{bio}$, and $GR2_{ab}$ decrease by a factor of ~20%, 30%-50%, and
370 60%-70%, respectively (Table 1). GR reactivity at alkaline pH can be ranked as: $GR1_{ab+P}$ >
371 $GR1_{bio}$ > $GR2_{ab}$. No significant difference in k_{obs} values was noted for each type of GRs
372 between pH 8.2 and 9.5 (Table 1). Thus, the reduction of $Hg(OH)_2$ by GR would be favored
373 at pH < 8.3 (Fig. 4). Therefore, the fluctuation of the surface charge of GR in the function of
374 pH governs the adsorption of $Hg(OH)_2$ and its reduction.

375 Coupled with the adsorption/reduction of $Hg(OH)_2$, a decrease in pH was observed for
376 the reaction with $GR2_{ab}$, whereas pH values remained almost constant with $GR1_{bio}$/$GR1_{ab+P}$
377 (Table S4). These observations are consistent with equations (5) and (6), since the reduction
378 of Hg^{II} is associated with the production of two H^+ for GR2 instead of one H^+ for GR1 (due to
379 the presence of bicarbonate at the pH range values investigated).

380 **4.2.3. Minor impact of cells and phosphate on the Hg^{II} reduction**

381 Phosphate and bacterial cells (as bacterial bodies with polymeric substances) are known
382 to improve the stability of GRs (Bocher *et al.*, 2004; Jorand *et al.*, 2013) and to affect their
383 reactivity towards nitrate (Etique *et al.*, 2014b; Zegeye *et al.*, 2014). To test whether these
384 stabilizing agents would affect the reactivity of the studied GRs towards Hg^{II}, experiments
385 were performed with and without bacterial cells or phosphate, and the rate and the extent of
386 the Hg^{II} reduction were determined. When $GR2_{ab}$ was supplemented with *S. putrefaciens* cells
387 ($GR2_{ab+cells}$), k_S did not significantly change compared to $GR2_{ab}$ (Fig. 2, Table 1). Similarly,
388 no significant difference was noted between $GR1_{ab}$ and $GR1_{ab+P}$ (*i.e.* GR1 supplemented with
389 0.8% phosphate) (Fig. 2b, Table 1). Therefore, bacterial cells or phosphates have a minor
390 impact on the reactivity of GRs towards Hg^{II}, and the $GR1_{bio}$ can reduce Hg^{II} as effectively as
391 $GR1_{ab}$. This suggests that *S. putrefaciens* did not inhibit significantly the reduction of Hg^{II} by
392 GRs as it has already been shown for other bacteria (Mishra *et al.*, 2011).

4.3. Kinetics of methyl red reduction by GRs

Here also, the reaction kinetics can be described by a pseudo first-order reaction (equations 10, 11):

$$d[MR]_t/dt = -k_{obs} \times [MR]_t \quad (10)$$

$$[MR]_t = [MR]_0 \times \exp(-k_{obs} \times t) \quad (11)$$

where k_{obs} is the pseudo first-order rate constant (min^{-1}), and $[MR]_t$ and $[MR]_0$ the total concentrations of MR at time *t* and *0*, respectively. However, it should be noted that a certain number of kinetic curves present a latency time (slight sigmoidal shape) ($GR1_{ab+Si}$ and $GR1_{ab+paa}$, Fig. 5), and a better description of this lag-time merits to be investigated in further studies.

The values of k_{obs} were determined from equation (11) by plotting $-\ln([MR]_t/[MR]_0)$ as a function of time *t* (Table 2). The Fe^{II} content of GRs and the concentration of Fe^{II} sites on the green rust surface were also taken into account to normalize k_{obs} values and to define $k_{Fe^{II}}$ (L min^{-1} $mmol^{-1}$) and k_S (L $mmol^{-1}$ min^{-1}), but it does not significantly affect the hierarchy as regards the kinetic rate constants (Table 2).

MR was completely reduced by $GR2_{ab}$ in less than 30 min with a k_S value of 3.4 L $mmol^{-1}$ min^{-1} ($t_{½}$ = 5 min) (Fig. 5). Generally, all the GRs used showed lower k_S values than those obtained for Hg^{II} reduction (except for the Hg^{II}/GR ratios of 1/10, 1/8 and 1/0.8). For example, MR was fully reduced by $GR1_{ab}$ in 120 min (Fig. 5) instead of only 60 min for a total reduction of Hg^{II} (Hg^{II}/GR ratio of 1/100) (Fig. 2a). However, k_S obtained for a reaction of MR with $GR1_{bio}$ had a significantly lower value (0.057 L $mmol^{-1}$ min^{-1}) (Table 2) when compared to the reaction between $GR1_{bio}$ (1/80) and Hg^{II} (k_{obs} = 1.18 $mmol^{-1}$ min^{-1}) (Table 1). Thus, the time needed to reduce MR by $GR1_{bio}$ (1200 min) (Fig. 5) is 20 times higher than for the reduction of Hg^{II} (60 min) (Fig. 2a).

4.3.1. Critical role of bacterial cells and phosphate on MR reduction

Since *Shewanella* spp. were shown to degrade MR (Khalid *et al.*, 2008), the degradation of MR by $GR1_{bio}$ could be due to an active metabolism of cells involved in the $GR1_{bio}$ formation and remaining in the mineral suspension. To assess the effect of *S. putrefaciens* on MR removal, a series of batch experiments were performed with a fresh cell suspension in the same physiological state (late stationary phase), and with a heat inactivated suspension. In both cases, no significant decrease in MR levels was obtained indicating that cells present with GR_{bio} do not contribute to MR removal (Fig. S5b).

To test whether bacteria could affect the reactivity of GRs, *Shewanella* cells were added to $GR2_{ab}$, the most reactive GR (high k_S). A significant decrease in the MR reduction rate by a factor of 200 was observed relative to $GR2_{ab}$ (Table 2, Fig. 5), which indicates that bacterial cells inhibit considerably the MR reduction by GRs. Similarly, k_S of $GR1_{ab+P}$ was ~200 times lower than that of $GR2_{ab}$ (0.007 L $mmol^{-1}$ min^{-1} and 3.4 L $mmol^{-1}$ min^{-1}, respectively, Table 2), thereby underscoring that phosphates impaired significantly the reactivity of GR. This is in line with a recent work dealing with the effect of phosphates on the reduction of nitrate by GR (Etique *et al.*, 2014b).

4.3.2. A moderate inhibition of GRs reactivity towards MR by silicate and polyacrylic acid

To investigate whether other environmentally relevant components could affect GR reactivity, experiments were performed with H_4SiO_4 and paa. Such compounds can represent (or be models of) aqueous Si from quartz associated with soil particles or extra-cellular polymeric substances from biofilms (Sergent *et al.*, 2011; Jorand *et al.*, 2013). The k_S of $GR1_{ab+Si}$ and $GR1_{ab+paa}$ (0.156 L $mmol^{-1}$ min^{-1} and 0.193 L $mmol^{-1}$ min^{-1}, respectively) were ~20 times higher than that of $GR1_{ab+P}$ and ~10 times lower than that of $GR2_{ab}$ (Table 2, Fig. 5). This result is in line with a recent study pointing out that GR1 stabilized with EPS ($GR1_{ab+paa}$) is quasi-unreactive towards nitrate (Zegeye *et al.*, 2014). Thus, it implies that paa,

443 H_4SiO_4, and cells would have a less pronounced "screen effect" than phosphate, or be sorbed
444 onto different reactive sites as compared to MR.

445 As stated before, the stoichiometric difference (Fe^{II}/Fe^{III}) between GRs could influence
446 the rate of reduction, as well as the concentration of surface Fe^{II} site of GR. However, even
447 considering k_s or k_{FeII}, the hierarchy of GR reactivity with MR remains unchanged (Table 2):
448 $k_S(GR1_{ab+P}) < k_S(GR2_{ab+cells}) < k_S(GR1_{bio}) < k_S(GR1_{ab+Si}) < k_S(GR1_{ab+paa}) < k_S(GR1_{ab}) < k_S(GR2_{ab})$.

449 To know whether MR was effectively reduced and not only sorbed onto the solid phase,
450 the presence of degradation products from MR reduction was checked. At the end of the
451 reduction, the main absorption peak at 430 nm had disappeared while a band in the ultraviolet
452 region at 305 nm had increased (Fig. S1). This absorbance band in the UV region could be
453 assigned to the presence of *p*-dimethylaminoaniline. This result is consistent with equation (5),
454 as well as with the findings of Hou *et al*. (2007) and Kone *et al*. (2009) who reported that
455 methyl orange and methyl red were reduced by zero-valent iron and $GR2_{ab}$, respectively,
456 through cleavage of the azo bond into sulfanilic or carboxyanilic acid and *p*-
457 dimethylaminoaniline. Control with aqueous Fe^{II} was performed and no reduction of MR was
458 observed (Fig. S5b).

459 **4.4. MR and Hg^{II} reduction mechanisms by GRs**

460 **4.4.1. Estimation of the number of moles of contaminant that could be reduced by GRs**

461 The number of moles of Hg^{II} species or MR that could be reduced for a given surface
462 area of GR at the given pH value can only be determined for a run highlighting an incomplete
463 consumption of the contaminant. Thus, the initial concentration of GR used during the
464 reduction of the pollutant has not to be sufficient to fully reduce the initial amount of Hg^{II}
465 species or MR. This phenomenon is described by the term saturation.

466 Additional experiment was carried out, where Hg^{II} species were added successively to
467 the $GR1_{bio}$ suspension (400 µM) in quantities of 5 µM to 100 µM to reach a final Hg^{II}

concentration of 130 µM in the reaction medium (pH 8.2) (Fig. 6). One day after the beginning of the reaction, the quantity of Hg^{II} removed was 77 µM (Fig. 6), representing 59 % of the total addition of Hg^{II}. Between each addition of Hg^{II}, the kinetics of the reaction decreased (first addition: $k_{obs,\#1} = 4.1 \pm 0.1 \times 10^{-2}$ min^{-1}; third addition: $k_{obs,\#3} = 1.6 \pm 0.2 \times 10^{-2}$ min^{-1}; last addition: $k_{obs,\#5} = 5.0 \times 10^{-4}$ min^{-1}) suggesting that the availability of Fe^{II} sites on the surface of $GR1_{bio}$ lowered. However, all the Fe^{II} sites on the $GR1_{bio}$ surface do not seem to be saturated with a Hg^{II}/GR ratio of 1/5.2 (i.e. 77/400). This ratio was increased in another additional run performed with a Hg^{II}/GR ratio of 1/0.8 at pH 8.2. A plateau was reached at 1.66 µM (Fig. S4b), evidencing a partial reduction of mercury with an initial concentration of $GR1_{bio}$ of 4 µM. Here, a saturation was highlighted and the amount of Hg^{II} species reduced by surface area concentration of $GR1_{bio}$ was estimated at 1.1×10^{-4} moles of Hg^{II} m^{-2}.

For the reduction of MR, none of our carried out experiments showed an incomplete consumption of $C_{15}H_{15}N_2O_3$ species at pH 7 (Fig. 5). Nevertheless, we can estimate the minimum amount of $C_{15}H_{15}N_2O_3$ species that can be reduced by $GR1_{bio}$ at 4.3×10^{-6} moles of MR m^{-2} or more.

4.4.2. Parameters influencing the kinetics of the MR reduction *vs* the Hg^{II} reduction

The MR reaction kinetics were more affected in the presence of GR stabilizing agents, such as phosphate or bacterial cells, than the reduction of Hg^{II} ($GR2_{ab+P}$/Hg^{II} and $GR2_{ab+cells}$/Hg^{II}, Fig. 2a; $GR2_{ab+P}$/MR and $GR2_{ab+cells}$/MR, Fig. 5). These stabilizing compounds have already proved their ability to prevent the formation of magnetite from $GR1_{ab}$ or $GR1_{bio}$ dissolution (Bocher *et al.*, 2004; Jorand *et al.*, 2013). It was suggested that reactive ferrous sites involved in GR dissolution and located on the lateral faces would be hidden by phosphate (Bocher *et al.*, 2004). For example, the reduction of nitrate by GR1 implies these lateral Fe^{II} sites, and its kinetics is strongly affected by phosphate (Etique *et al.*, 2014b), by EPS (Zegeye *et al.*, 2014), or by silicate (data not shown). In the present

investigation, since GR stabilizing agents affect MR reduction, MR would preferentially react with the same Fe^{II} sites of GR as those involved by the sorbing ligands. As Hg^{II} reduction was slightly affected by phosphate or cells, we may suppose that Hg^{II} would preferentially react with other reactive sites, which might rather be located on the basal face of the GR crystal. Other GR stabilizers such as silicate and paa, are also known to prevent unstable GRs from transforming into magnetite (Sergent *et al.*, 2011; Jorand *et al.*, 2013), however, they affect to a lesser degree the MR reduction by GRs.

In addition, the presence of sorbing ligands could slow down the reactivity of GRs by electrostatic repulsion and/or steric hindrance. Indeed, the interactions of negatively charged MR with GR surfaces covered with a layer of anionic ligands such as phosphate anions, cells, or polymers might also explain the decrease in the reduction rate of MR as compared to that of Hg.

5. Conclusion

The difference in reactivity between GRs has more to do with the nature of the contaminant (Hg^{II} or MR) than with the type of GRs (GR1 or GR2). At pH 7, the reaction of GRs with MR is generally slower than with Hg^{II}, and moreover, the reduction of MR seems to be more affected by stabilizing agents than Hg^{II} reduction. More precisely, the reduction of MR is sharply limited by phosphate and bacterial cells, whereas in the presence of silicate and paa this reduction is moderate. This difference in GR reactivity towards mercury and methyl red would probably be based on the nature of Fe^{II} surface sites involved during the reduction: lateral Fe^{II} surface sites would be monopolized for MR reduction, whereas basal Fe^{II} surface sites would interact with Hg^{II} species.

Although the Hg^{II} reduction is slightly hindered in the presence of stabilizing agents, the variation of pH suspension from 7.0 to 9.5 leads to a decrease of the kinetics rate. This finding can be explained by the fluctuation of the surface charge of GR (pH 7.0: positive, pH

8.2: zero, pH 9.5: negative) that governs the adsorption and the reduction of $Hg(OH)_2$, the predominant phase of Hg^{II} species at pH of this investigation.

In environmental conditions where the fougèrite mineral can be represented by biologically synthesized hydroxycarbonate green rust ($GR1_{bio}$), Hg^{II} species would be more reduced than MR. Indeed, the amount of Hg^{II} species reduced by surface area of $GR1_{bio}$ (1.1×10^{-4} moles of Hg^{II} m^{-2}) is significantly higher than those of MR (4.3×10^{-6} moles of MR m^{-2}). In engineering applications using GRs as a reactive sorbent and/or reducing agent, more attention should be paid to the co-occurring ligands as regards the type of target pollutants. These results have strong implications in attenuation and remediation studies aiming to predict the fate and transport of methyl red and mercury in natural or engineered systems.

Acknowledgements

The authors acknowledge financial support from the Agence Nationale de la Recherche (France) ("Arctic Metals" project), the Ministère de l'Enseignement Supérieur et de la Recherche (France), and the Zone Atelier Moselle (Lorraine, France). We thank J. Ghanbaja for TEM analysis, I. Bihannic for XRD analysis, B. Grégoire and A. Razafitianamaharavo for BET analysis, and M. Abdelmoula for TMS analysis.

List of symbols

$GR1_{ab}$: abiotically synthesized hydroxycarbonate green rust

$GR2_{ab}$: abiotically synthesized hydroxysulfate green rust

$GR1_{bio}$: microbially synthesized hydroxycarbonate green rust

$GR1_{ab+P}$: abiotically synthesized hydroxycarbonate green rust with phosphate

$GR1_{ab+Si}$: abiotically synthesized hydroxycarbonate green rust with silicic acid

$GR1_{ab+paa}$: abiotically synthesized hydroxycarbonate green rust with polyacrylic acid

543 $GR2_{ab+cells}$: abiotically synthesized hydroxysulfate green rust with heat-killed cells

544 A: surface area concentration (m^2 L^{-1})

545 k_{obs}: pseudo first-order rate constant (min^{-1})

546 k_{FeII}: k_{obs} normalized to the Fe^{II} content of GRs (L $mmol^{-1}$ min^{-1})

547 k_s: k_{obs} normalized to the estimated Fe^{II} surface sites of GRs (L $mmol^{-1}$ min^{-1})

548 paa: polyacrylic acid

549

550 Appendix A. Supplementary data

551 Supplementary data associated with this article (Tables S1 – S4; Notes S1 – S3; and Fig. S1 –

552 S6) can be downloaded online.

553

554 References

555 Bearcock, J. M., Perkins, W. T., Pearce, N. J. G., 2011. Laboratory studies using naturally

556 occurring "green rust" to aid metal mine water remediation. Journal of Hazardous

557 Materials 190, 466–473.

558 Benali, O., Abdelmoula, M., Refait, P., Génin, J.-M. R. 2001. Effect of orthophosphate on the

559 oxidation products of Fe(II)–Fe(III) hydroxycarbonate: the transformation of green rust to

560 ferrihydrite. Geochimica et Cosmochimica Acta 65, 1715–1726.

561 Bocher, F., Géhin, A., Ruby, C., Ghanbaja, J., Abdelmoula, M., Génin J-M. R. 2004.

562 Coprecipitation of Fe(II–III) hydroxycarbonate green rust stabilized by phosphate

563 adsorption. Solid State Sciences 6 (1), 117–124.

564 Carlson, H. K., Clark, I. C., Melnyk, R. A., Coates, J. D. 2012. Toward a mechanistic

565 understanding of anaerobic nitrate-dependent iron oxidation: balancing electron uptake and

566 detoxification. Frontiers in Microbiology 3 (57), 1–6.

567 Charlet, L., Bosbach, D., Peretyashko, T. 2002. Natural attenuation of TCE, As, Hg linked to
568 the heterogeneous oxidation of Fe(II): an AFM study. Chemical Geology 190, 303–319.
569 Christiansen, B. C., Balic-Zunic, T., Dideriksen, K., Stipp, S. L. S. 2009. Identification of
570 green rust in groundwater. Environmental Science & Technology 43, 3436–3441.
571 Drissi, S. H., Refait, P., Abdelmoula, M., Génin, J.-M. R. 1995. The preparation and
572 thermodynamic properties of iron(II)-iron(III) hydroxide-carbonate (green rust); Pourbaix
573 diagram of iron in carbonate-containing aqueous media. Corrosion Science 37, 2025–2041.
574 Elsner M., Schwarzenbach R. P., Haderlein, S. B. 2004. Reactivity of Fe(II)-bearing minerals
575 toward reductive transformation of organic contaminants. Environmental Science &
576 Technology 38, 799–807.
577 Erbs, M., Hansen, H. S. B., Olsen, C. E. 1999. Reductive dechlorination of carbon
578 tetrachloride using iron(II) iron(III) hydroxide sulfate (green rust). Environmental Science
579 & Technology 33, 307–311.
580 Etique, M., Jorand, F. P. A., Zegeye, A., Grégoire, B., Despas, C., Ruby, C. 2014a. Abiotic
581 process for Fe(II) oxidation and green rust mineralization driven by a heterotrophic nitrate
582 reducing bacteria (*Klebsiella mobilis*). Environmental Science & Technology 48,
583 3742−3751.
584 Etique, M., Zegeye, A., Grégoire, B., Carteret, C., Ruby, C. 2014b. Nitrate reduction by
585 mixed iron(II-III) hydroxycarbonate green rust in the presence of phosphate anions: the
586 key parameters influencing the ammonium selectivity. Water Research 62, 29–39.
587 Fredrickson, J. K., Zachara, J. M., Kennedy, D. W., Dong, H., Onstott, T. C., Hinman, N. W.,
588 Li, S.-M. 1998. Biogenic iron mineralization accompanying the dissimilatory reduction of
589 hydrous ferric oxide by a groundwater bacterium. Geochimica et Cosmochimica Acta 62,
590 3239–3257.

591 Génin, J.-M. R., Abdelmoula, M., Ruby, C., Upadhyay, C. 2006. Speciation of iron;
592 characterisation and structure of green rusts and Fe^{II-III} oxyhydroxycarbonate fougerite.
593 Comptes Rendus Geosciences 338, 402-419.
594 Génin, J.-M. R., Bourrié, G., Trolard, F., Abdelmoula, M., Jaffrezic, A., Refait, P., Maître, V.,
595 Humbert, B., Herbillon, A. 1998. Thermodynamic equilibria in aqueous suspensions of
596 synthetic and natural Fe(II)–Fe(III) green rusts: occurrences of the mineral in
597 hydromorphic soils. Environmental Science & Technology 32, 1058–1068.
598 Guilbaud, R., White, M. L., Poulton, S. W. 2013. Surface charge and growth of sulphate and
599 carbonate green rust in aqueous media. Geochimica et Cosmochimica Acta 108, 141-153.
600 Hansen, H. C. B., Guldberg, S., Erbs, M., Koch, C.-B. 2001. Kinetics of nitrate reduction by
601 green rusts effects of interlayer anion and Fe(II):Fe(III) ratio. Applied Clay Sciences 18,
602 81–91.
603 Hou, X.-L., Yang ,Z., Yeung, K.-S., Wong, H. N. C., 2007. Chapter 5.3 Five-membered ring
604 systems: furans and benzofurans. Progress in Heterocyclic Chemistry 18, (C), 187–217.
605 Jorand, F. P. A, Sergent, A.-S., Remy, P.-P., Bihannic, I., Ghanbaja, J., Lartiges, B., Hanna,
606 K., Zegeye, A. 2013. Contribution of anionic *vs* neutral polymers to the formation of green
607 rust 1 from γ-FeOOH bioreduction. Geomicrobiology Journal 30, 600–615.
608 Khalid, A., Arshad, M., Crowley, D. E. 2008. Decolorization of azo dyes by *Shewanella* sp.
609 under saline conditions. Applied Microbiology and Biotechnology 79, 1053-1059.
610 Kone, T., Hanna, K., Abdelmoula, M., Ruby, C., Carteret, C., 2009. Reductive transformation
611 and mineralization of an azo dye by hydroxysulphate green rust preceding oxidation using
612 H_2O_2 at neutral pH. Chemosphere 75, 212–219.
613 Lee, W., Batchelor, B., 2002. Abiotic reductive dechlorination of chlorinated ethylenes by
614 iron-bearing soil minerals. 2. Green rust. Environmental Science & Technology 36, 5348-
615 5354.

616 Loyaux-Lawniczak, S., Refait, P., Ehrhardt, J.-J., Lecomte, P., Génin, J.-M. R., 2000.
617 Trapping of Cr by formation of ferrihydrite during the reduction of chromate ions by
618 Fe(II)-Fe(III) hydroxysalt green rusts. Environmental Science & Technology 34, 438-443.
619 Mills, S. J., Christy, A. G., Génin, J.-M. R., Kameda, T., Colombo, F., 2012. Nomenclature of
620 the hydrotalcite supergroup: natural layered double hydroxides. Mineralogical Magazine
621 76, 1289-1336.
622 Mishra, B., O'Loughlin, E. J., Boyanov, M. I., Kemner, K. M., 2011. Binding of Hg^{II} to high-
623 affinity sites on bacteria inhibits reduction to Hg0 by Mixed $Fe^{II/III}$ phases. Environmental
624 Science & Technology 45, 9597–9603.
625 Mitsunobu, S., Takahashi, Y., Sakai, Y., 2008. Abiotic reduction of antimony (V) by green
626 rust ($Fe_4(II)Fe_2(III)(OH)_{12}SO_4 \cdot 3H_2O$). Chemosphere 70, 942–947.
627 Myneni, S. C. B., Tokunaga, T. K., Brown Jr., G. E., 1997. Abiotic Se redox chemistry in the
628 presence of Fe(II, III)-oxides. Science 278, 1106 – 1109.
629 O'Loughlin, E. J., Burris, D. R., 2004. Reduction of halogenated ethanes by green rust.
630 Environmental Toxicology and Chemistry 23, 41-48.
631 O'Loughlin, E. J., Kelly, S. D., Kemner, K. M., Csencsits R., Cook, R. E. 2003. Reduction of
632 Ag^{I}, Au^{III}, Cu^{II}, and Hg^{II} by Fe^{II}/Fe^{III} hydroxysulfate green rust. Chemosphere 53, 437-446.
633 O'Loughlin, E. J., Gorski C. A., Scherer M. M., Boyanov M. J., Kemner K. M. 2010. Effects
634 of oxyanions, natural organic matter, and bacterial cell numbers on the bioreduction of
635 lepidocrocite (γ-FeOOH) and the formation of secondary mineralization products.
636 Environmental Science & Technology 44, 4570-4576.
637 Ona-Nguema, G., Abdelmoula, M., Jorand, F., Benali, O., Géhin, A., Block, J.-C., Génin J.-M.
638 R., 2002. Iron (II, III) hydroxycarbonate green rust formation and stabilization from
639 lepidocrocite bioreduction. Environmental Science & Technology 36, 16-20.

640 Pasakarnis, T. S., Boyanov, M. I., Kemner, K. M., Mishra, B., O'Loughlin, E. J., Parkin, G.,
641 Scherer, M. M., 2013. Influence of chloride and Fe(II) content on the reduction of Hg(II)
642 by magnetite. Environmental Science & Technology 47, 6987-6994.
643 Pourbaix, M., 1963. Atlas d'équilibres électrochimiques. Gauthier-Villars et Cie, Paris, pp.
644 422-427.
645 Refait, P., Memet, J.-B., Bon, C., Sabot, R., Génin, J.-M. R., 2003. Formation of the Fe(II)–
646 Fe(III) hydroxysulphate green rust during marine corrosion of steel. Corrosion Science 45,
647 833-845.
648 Refait, P., Abdelmoula, M., Génin, J.-M. R., Sabot, R., 2006. Green rusts in electrochemical
649 and microbially influenced corrosion of steel. Comptes Rendus Geosciences 338, 476-487.
650 Ruby, C., Géhin, A., Abdelmoula, M., Génin, J.-M. R., Jolivet, J. P., 2003. Coprecipitation of
651 Fe(II) and Fe(III) cations in sulphated aqueous medium and formation of hydroxysulphate
652 green rust. Solid State Sciences 5, 1055-1062.
653 Ruby, C., Haissa, R., Géhin, A., Abdelmoula, M., Génin, J.-M. R., 2006. Chemical stability
654 of hydroxysulphate green rust synthesized in the presence of foreign anions: carbonate,
655 phosphate and silicate. Hyperfine Interactions 167, 803-807.
656 Schwertmann, U., Fechter, H., 1994. The formation of green rust and its transformation to
657 lepidocrocite. Clay Minerals 29, 87-92.
658 Sergent, A.-S., Jorand, F., Hanna, K., 2011. Effects of Si-bearing minerals on the nature of
659 secondary iron mineral products from lepidocrocite bioreduction. Chemical Geology 289,
660 86–97.
661 Simon L., Francois M., Refait P., Renaudin G., Lelaurain M., and Génin J.-M. R., 2003.
662 Structure of the Fe(II-III) layered double hydroxysulphate green rust two from Rietveld
663 analysis. Solid State Sciences 5, 327–334.

664 Su, C, Puls, R. W., 2004. Significance of iron(II,III) hydroxycarbonate green rust in arsenic
665 remediation using zerovalent iron in laboratory column tests. Environmental Science &
666 Technology 38, 5224-5231.
667 Taylor, R. M.,Schwertmann, U., Fechter, H., 1985. A rapid method for the formation of
668 Fe(II)-Fe(III) hydroxycarbonate. Clay Minerals 20, 147–151.
669 Viollier, E., Inglett, P. W., Hunter, K., Roychoudhury, A. N., Van Cappellen, P. 2000. The
670 ferrozine method revisited: Fe(II)/Fe(III) determination in natural waters. Applied
671 Geochemistry 15, 785-790.
672 Wiatrowski, H. A., Das, S., Kukkadapu, R., Ilton, E. S., Barkay, T., Yee, N. 2009. Reduction
673 of Hg(II) to Hg(0) by magnetite. Environmental Science & Technology 43, 5307–5313.
674 Wiatrowski, H. A., Ward, P. M., Barkay, T., 2006. Novel reduction of mercury(II) by
675 mercury-sensitive dissimilatory metal reducing bacteria. Environmental Science &
676 Technology 40, 6690–6696.
677 Williams, A., Scherer, M. M., 2001. Kinetics of Cr(VI) reduction by carbonate green rust.
678 Environmental Science & Technology 35, 3488–3494.
679 Zegeye, A., Bonneville, S., Benning, L. G., Sturm A., Fowle D. A., Jones, C. A., Canfield, D.
680 E., Ruby C., MacLean, L. C., Nomosatryo, S., Crowe, S. A., Poulton, S. W., 2012. Green
681 rust formation controls nutrient availability in a ferruginous water column. Geology 40,
682 599-602.
683 Zegeye, A., Etique, M., Carteret, C., Ruby, C., Schaaf, P., Francius, G., 2014 Origin of the
684 differential nanoscale reactivity of biologically and chemically formed green rusts crystals
685 investigated by chemical force spectroscopy. Journal of Physical Chemistry C 118, 5978–
686 5987.
687 Zegeye, A., Mustin, C., Jorand, F. 2010. Bacterial and iron oxide aggregates mediate
688 secondary iron mineral formation: green-rust vs magnetite. Geobiology 8, 209-22.

689 Zegeye, A., Ona-Nguema, G., Carteret, C., Huguet, L., Abdelmoula, M., Jorand, F., 2005.
690 Formation of hydroxysulphate green rust 2 as a single iron(II–III) mineral in microbial
691 culture. Geomicrobiology Journal 22, 389–399.
692 Zegeye, A., Ruby, C., Jorand, F., 2007. Kinetic and thermodynamic analysis during
693 dissimilatory γ-FeOOH reduction: formation of green rust 1 and magnetite.
694 Geomicrobiology Journal 24, 51-64.

Table 1. Kinetics rate constants (k_{obs}, min^{-1}), k_{obs} normalized to surface Fe^{II} sites (k_s, L $mmol^{-1}$ min^{-1}) and k_{obs} normalized to structural Fe^{II} (k_{FeII}, L $mmol^{-1}$ min^{-1}) of the reduction of Hg^{II} (5 µM) by chemically synthesized carbonated green rust ($GR1_{ab}$ or $GR1_{ab+P}$ supplemented with phosphate), biogenic carbonated green rust ($GR1_{bio}$), chemically synthesized sulfated green rust ($GR2_{ab}$), or $GR2_{ab}$ with a cell suspension ($GR2_{ab+cells}$). Each batch was conducted with 0.5 mM (Hg^{II}/GR = 1/100) or 0.05 mM (Hg^{II}/GR = 1/10) of GR in duplicates (except when specified). *A* = surface area concentration (m^2 L^{-1}). ND = not determined.

	A (m^2 L^{-1})	Structural Fe^{II} (mM)	Surface Fe^{II} sites (µM)	Hg^{II}/GR	Rate constants	pH 7.0 $\times 10^{-2}$	pH 8.2 $\times 10^{-2}$	pH 9.5 $\times 10^{-2}$
$GR1_{ab}$	10±2[a]	2.2	*83*	1/100	k_{obs}	ND	2.5 ± 0.3	ND
					k_s	*ND*	*30 ± 3*	*ND*
					k_{Fe}^{II}	*ND*	*1.1 ± 0.1*	*ND*
		0.22	8.3	1/10	k_{obs}	ND	8.6 ± 0.1	ND
					k_s	*ND*	*1036 ± 12*	*ND*
					k_{Fe}^{II}	*ND*	*39.1 ± 0.5*	*ND*
$GR1_{ab+P}$	10±2	1.2	83	1/100	k_{obs}	3.8 ± 0.2	3.0± 0.6	3.1 ± 0.2
					k_s	*45 ± 2*	*36 ± 7*	*37 ± 2*
					k_{Fe}^{II}	*3.2 ± 0.2*	*2.5 ± 0.5*	*2.6 ± 0.2*
$GR1_{bio}$	4.2	1.3	34.8	1/80	k_{obs}	4.1 ± 0.2	2.2 ± 0.3	2.7 ± 0.5
					k_s	*118 ± 6*	*63 ± 8*	*78 ± 14*
					k_{Fe}^{II}	*3.1 ± 0.1*	*1.7 ± 0.2*	*2.1 ± 0.4*
		0.13	3.48	1/8	k_{obs}	ND	3.5 ± 0.4	ND
					k_s	*ND*	*1006 ± 114*	*ND*
					k_{Fe}^{II}	*ND*	*27 ± 3*	*ND*
		0.013	0.348	1/0.8	k_{obs}	ND	1.5[b]	ND
					k_s	*ND*	*4310*	*ND*
					k_{Fe}^{II}	*ND*	*115*	*ND*
$GR2_{ab}$	4.6±0.7	2.0	38.2	1/100	k_{obs}	4.1 ± 0.2	1.6 ± 0.1	1.1[b]
					k_s	*107 ± 5*	*42 ± 2*	*29*
					k_{Fe}^{II}	*2.0 ± 0.1*	*0.80 ± 0.05*	*0.6*
$GR2_{ab+cells}$	4.6±0.7	2.0	38.2	1/100	k_{obs}	1.8 ± 0.4[c]	2.1 ± 0.5	2.8 ± 0.9
					k_s	*47 ± 11*	*55 ± 13*	*73 ± 24*
					k_{FeII}	*0.9 ± 0.2*	*1.05 ± 0.25*	*1.4 ± 0.5*

[a] Assuming the surface area was the same than $GR1_{ab+P}$
[b] n = 1
[c] n = 3 independent experiments

Table 2: Kinetics rate constants (k_{obs}), k_{obs} normalized to surface Fe^{II} (k_s, L $mmol^{-1}$ min^{-1}) and k_{obs} normalized to structural Fe^{II} (k_{FeII}, L $mmol^{-1}$ min^{-1}) of the reduction of methyl red (MR) by chemically synthesized carbonated green rust ($GR1_{ab}$), $GR1_{ab}$ supplemented with 4 mM phosphate ($GR1_{ab+P}$) or with 4 mM H_4SiO_4 ($GR1_{ab+Si}$) or with 0.5 g L^{-1} of polyacrylic acid ($GR1_{ab+paa}$) or by biogenic carbonated green rust ($GR1_{bio}$), chemically synthesized sulfated green rust ($GR2_{ab}$), or $GR2_{ab}$ supplemented with a cell suspension ($GR2_{ab+cells}$). All experiments were done at pH 7.0 ± 0.1 and in duplicates (except for $GR1_{ab+Si}$). *A* = surface area concentration.

	A (m^2 L^{-1})	Structural Fe^{II} (mM)	Surface Fe^{II} sites (µM)	MR/GR	$k_{obs}\times10^{-3}$ (min^{-1})	$k_s\times10^{-3}$ (L $mmol^{-1}$ min^{-1})	$k_{Fe^{II}}\times10^{-3}$ (L $mmol^{-1}$ min^{-1})
$GR1_{ab}$	10±2[a]	2.2	83	1/33	28 ± 4	337 ± 48	13 ± 2
$GR1_{ab+P}$	10±2	1.2	83	1/33	0.6 ± 0.1	7 ± 1	0.5 ± 0.1
$GR1_{ab+Si}$	10±2[a]	1.2	83	1/33	13[b]	156	11
$GR1_{ab+paa}$	10±2[a]	1.2	83	1/33	16[b]	193	13
$GR1_{bio}$	4.2	1.3	34.8	1/26	2.0 ± 0.2	57 ± 6	1.5 ± 0.1
$GR2_{ab}$	4.6±0.7	2.0	38.2	1/33	130 ± 50	3403 ± 1308	65 ± 25
$GR2_{ab+cells}$	4.6±0.7	2.0	38.2	1/33	0.6 ± 0.2	16 ± 5	0.3 ± 0.1

[a] Assuming the surface area was the same than $GR1_{ab+P}$
[b] n = 1

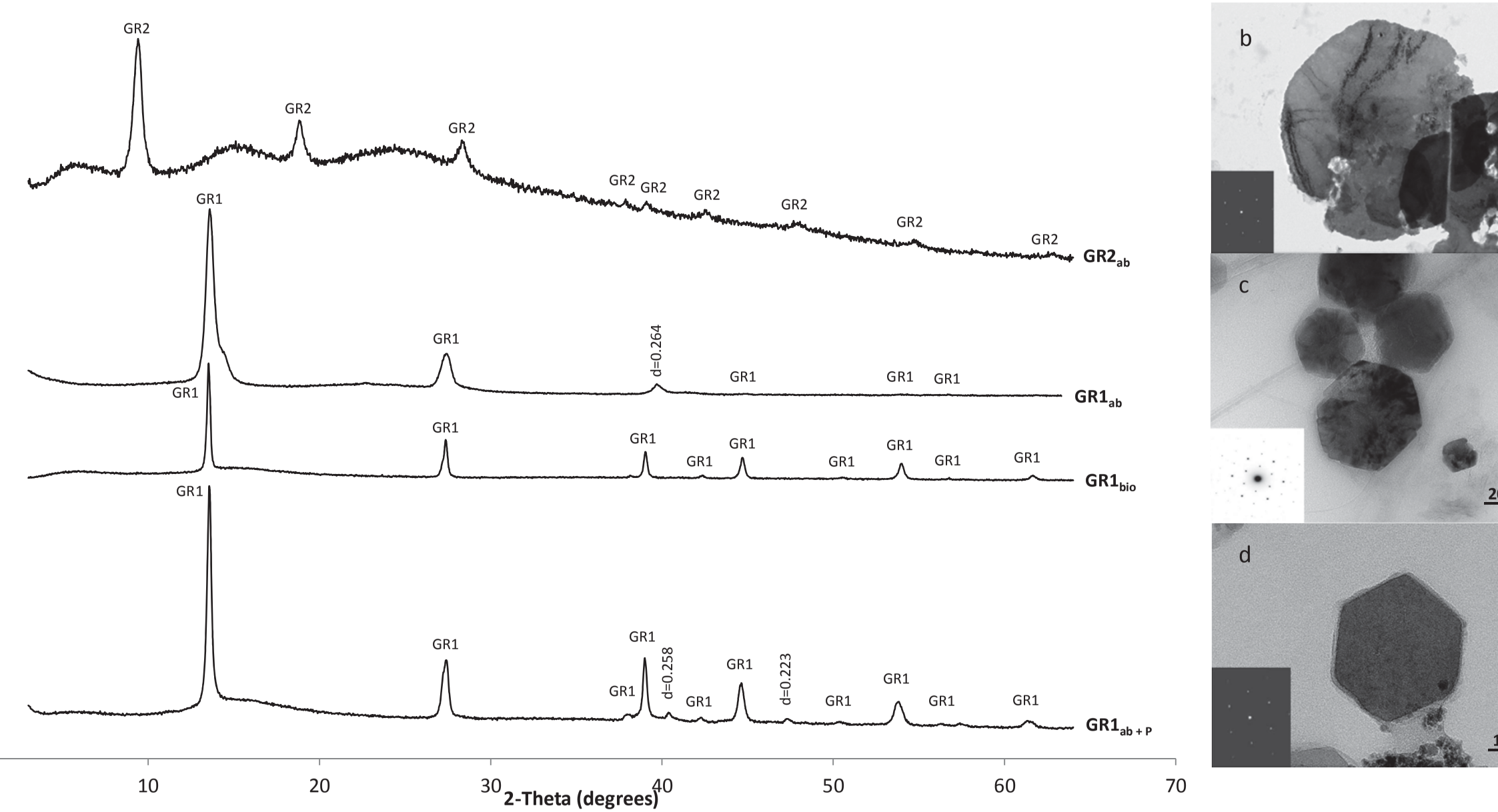

g. 1. X-ray diffractograms (Co, l = 0.178897 nm) of the biogenic carbonated green rust 1 after microbial reduction of lepidocrocite (γ-FeOOH) by *Shewanella putrefaciens* ($GR1_b$ emically synthesized carbonated green rust 1 ($GR1_{ab}$), chemically synthesized carbonated green rust 1 stabilized by phosphate ($GR1_{ab+P}$) and sulfated green rust 2 ($GR2_{ab}$) (a); T ages of $GR1_{bio}$, (b), $GR2_{ab}$ (c), and $GR1_{ab+P}$ (d) crystals. Inserts show the electron diffraction pattern of each GR. With $GR1_{ab+P}$, a few minor peaks (d = 0.186 nm; d = 0.223 nm; = 0.258 nm) were detected on XRD diffractogram (a), corresponding probably to chukanovite ($Fe_2(OH)_2CO_3$), but this phase was not confirmed by Mössbauer analysis.

a)

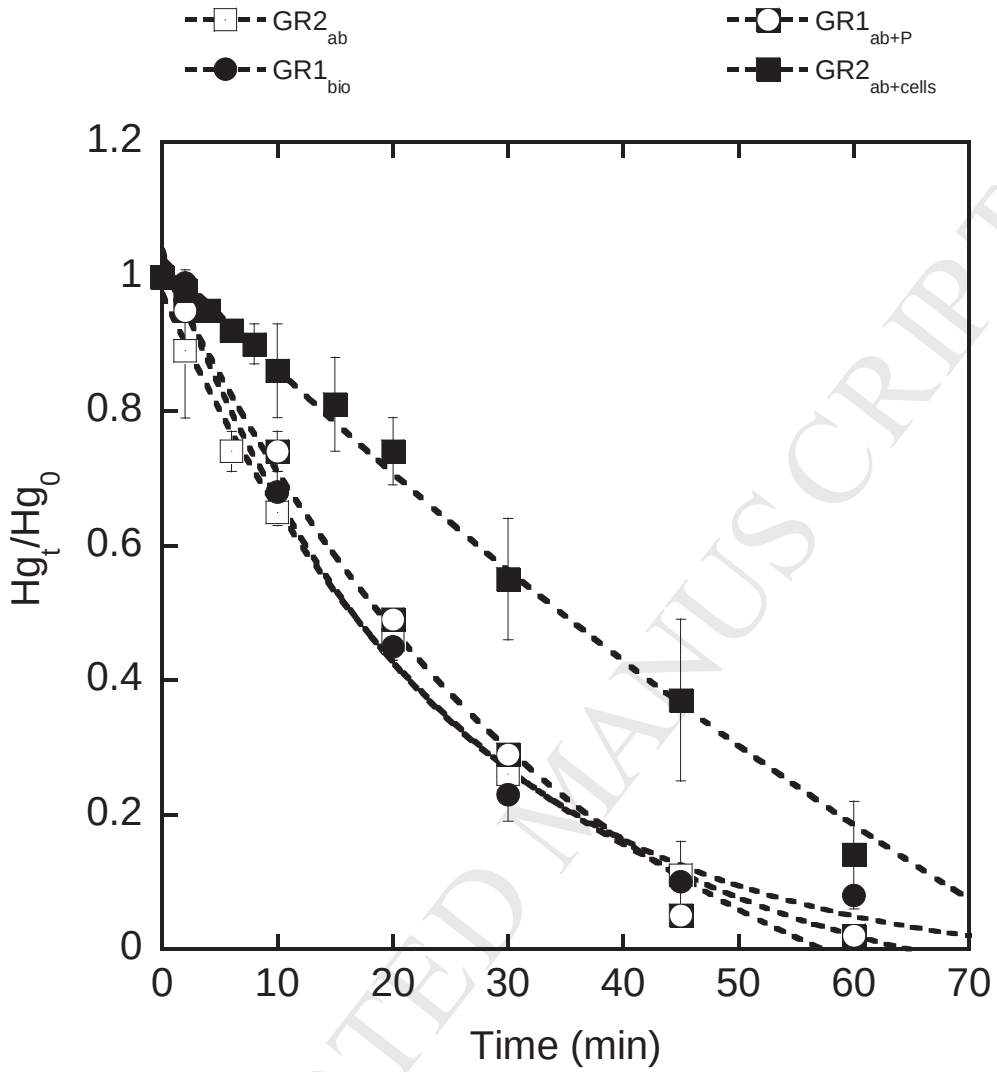

Fig 2a

b)

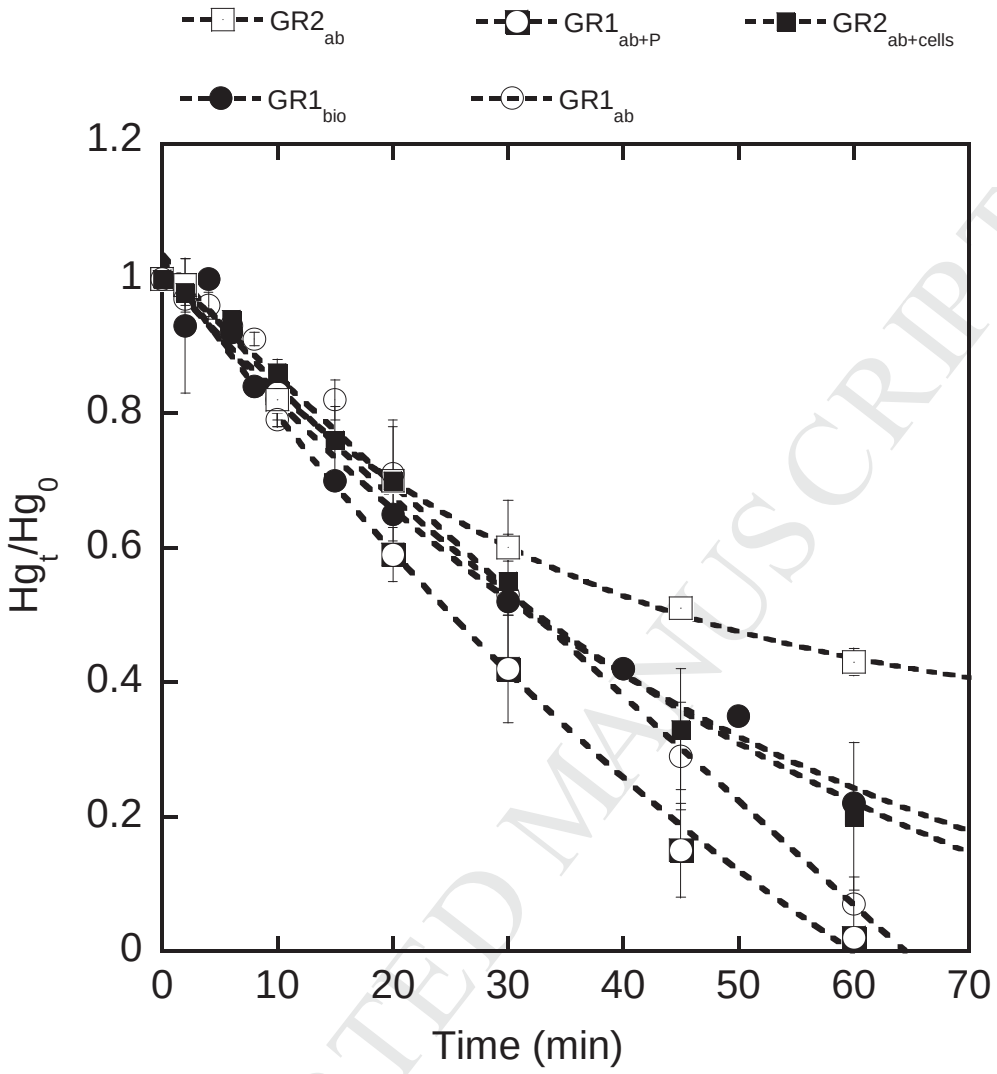

Fig 2b

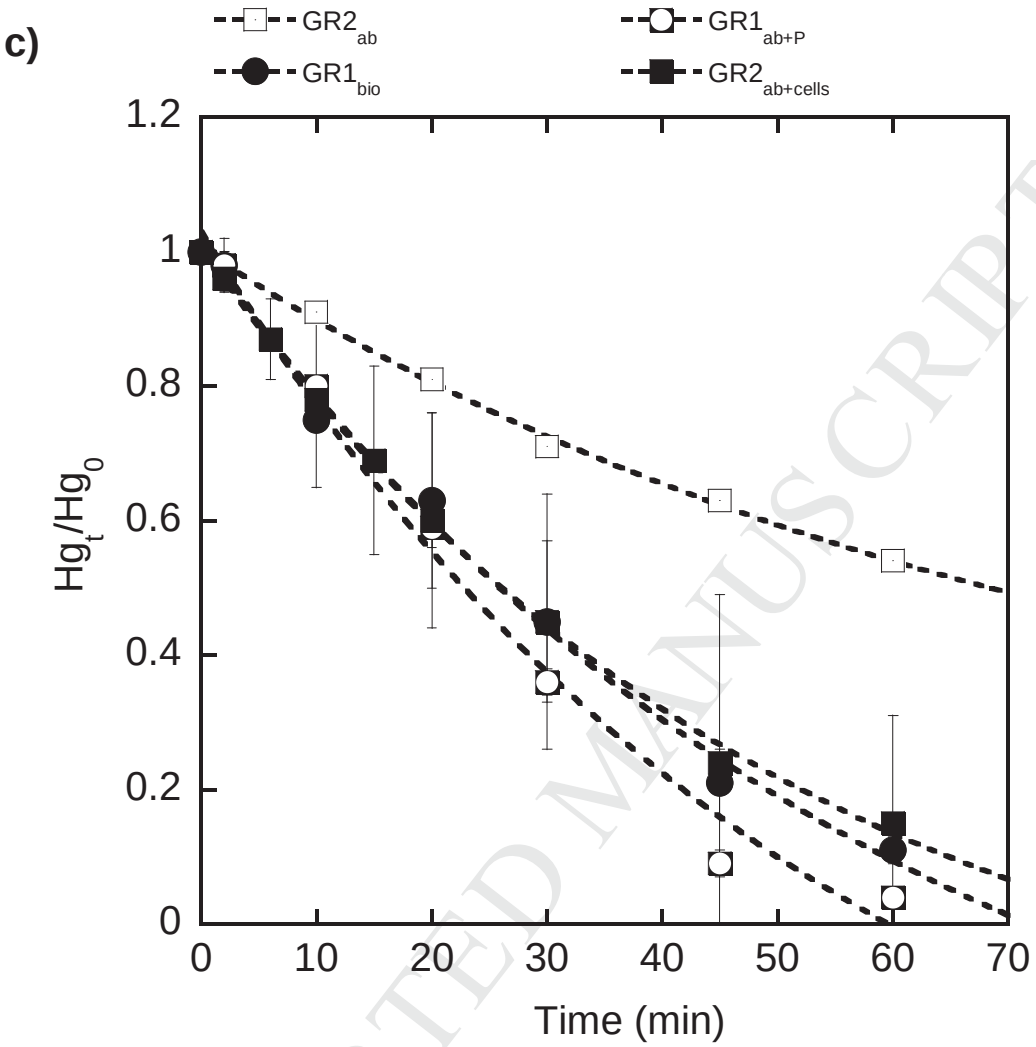

Fig. 2. Removal of mercury over time in the presence of green rusts: 400 µM of biologically synthesized hydroxycarbonate green rust ($GR1_{bio}$), and 500 µM of chemically synthesized hydroxycarbonate green rust ($GR1_{ab}$), $GR1_{ab}$ supplemented with phosphate ($GR1_{ab+P}$), hydroxysulfate green rust ($GR2_{ab}$) and $GR2_{ab}$ supplemented with cells ($GR2_{ab+cells}$). The amount of Hg remaining in solution (Hg_t/Hg_0) is plotted as a function of time at a pH of 7.0 ± 0.1 (a), 8.2 ± 0.1 (b), and 9.5 ± 0.1 (c). The changes in pH after a 60 h incubation time period are reported in Table S7. Bars are the errors of two independent experiments.

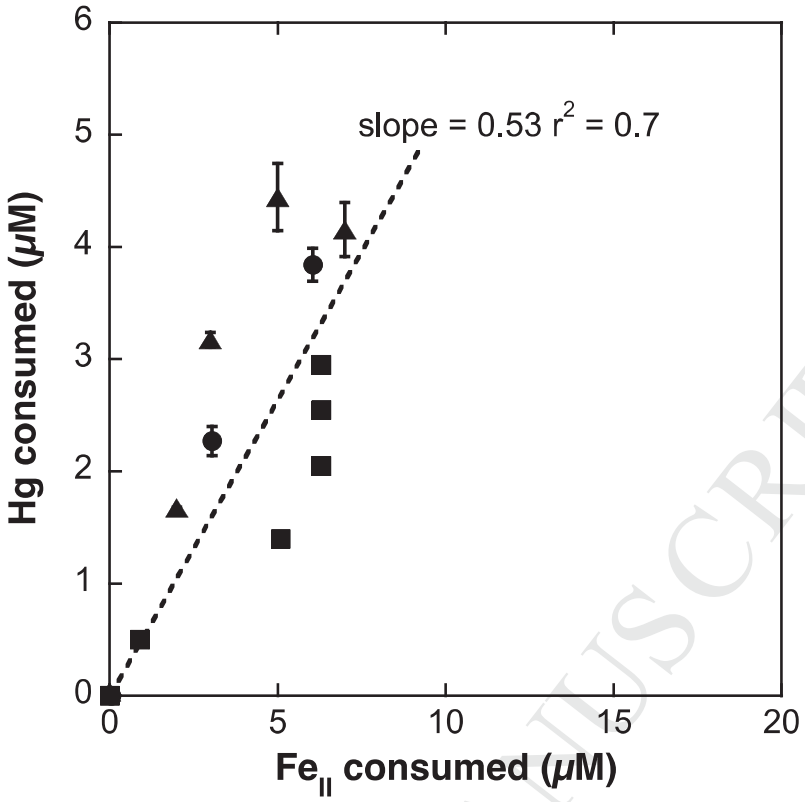

Fig. 3. Evolution of the mercury consumption as a function of the Fe^{II} consumption for time between 0 and 60 min with Hg^{II}/GR ratios of 1/10 for $GR1_{ab}$ (circle), 1/8 (triangle) and 1/0.8 (square) for $GR1_{bio}$. The slope of 0.53 fits well with the expected ratio Hg^{II}:Fe^{II}_{GR} of 1:2. Error bars were drawn for two independent assays.

1

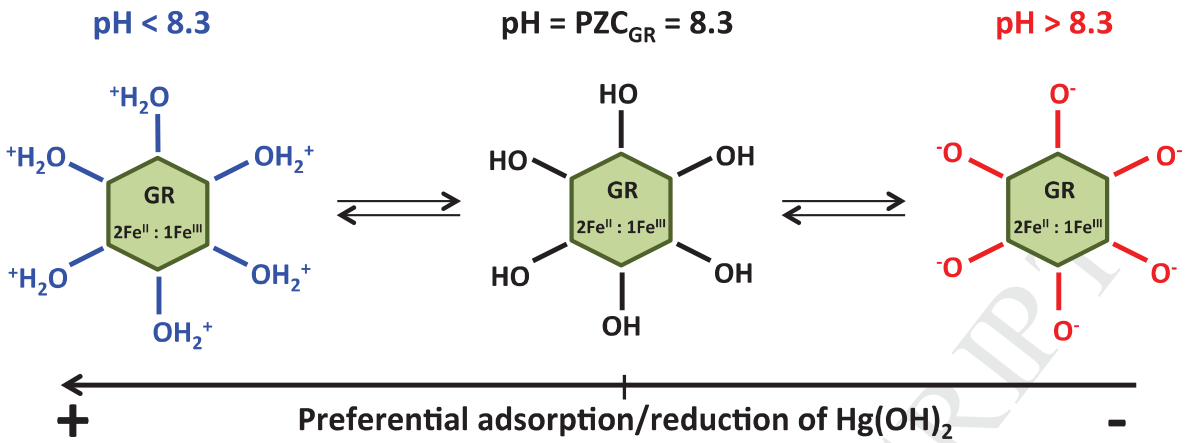

2

3

4 **Fig. 4**. – Green rust particles behavior at low/high pH and preferential adsorption/reduction of
5 $Hg(OH)_2$.

6

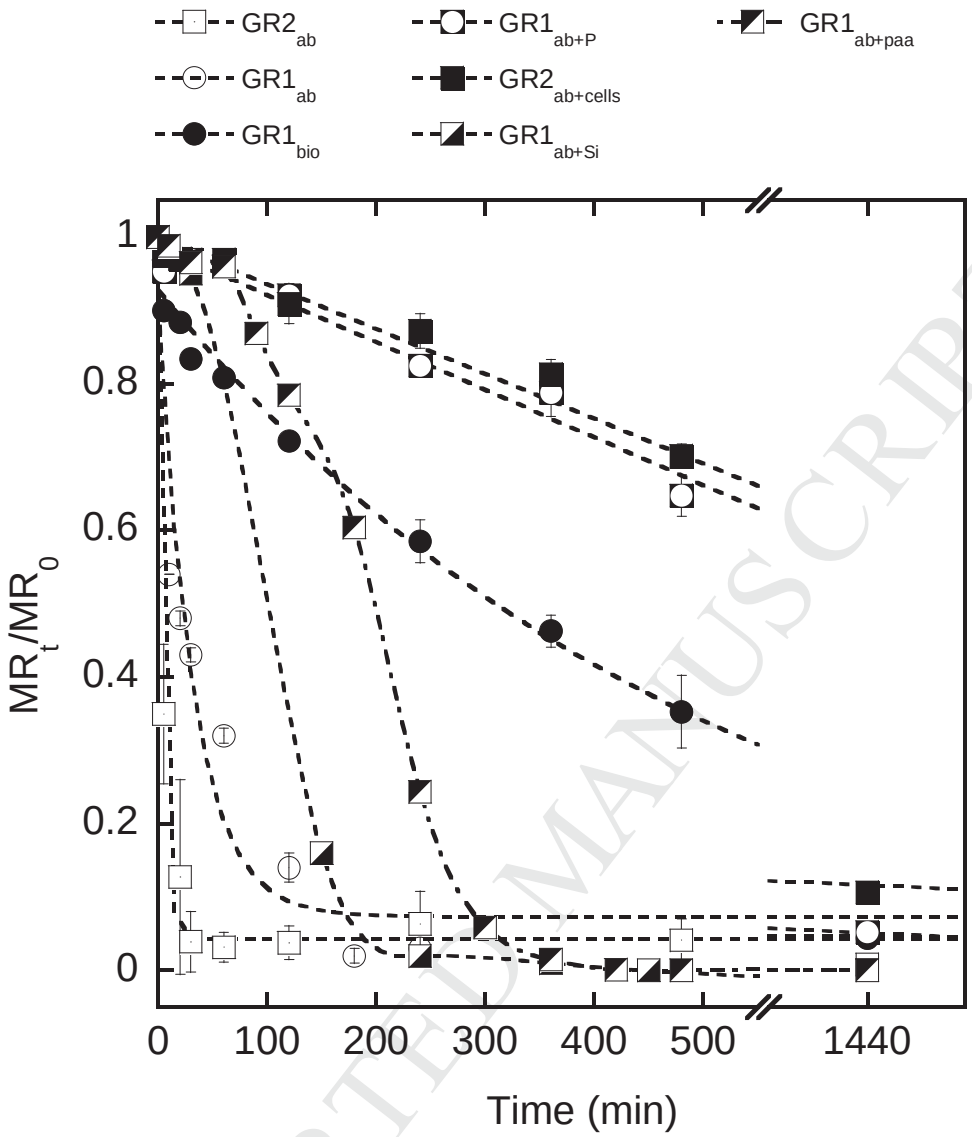

Fig. 5. Removal of methyl red (MR) in the presence of green rusts: 400 µM of biologically synthesized hydroxycarbonate green rust ($GR1_{bio}$), and 500 µM of chemically synthesized hydroxycarbonate green rust ($GR1_{ab}$), $GR1_{ab}$ supplemented with phosphate ($GR1_{ab+P}$), silicate ($GR1_{ab+Si}$), polyacrylic acid ($GR1_{ab+paa}$), hydroxysulfate green rust ($GR2_{ab}$) and $GR2_{ab}$ supplemented with cells ($GR2_{ab+cells}$). The MR remaining in solution (MR_t/MR_0) is plotted as a function of time. The pH was manually held at a constant value of 7.0 before each sampling by addition of HCl 1M or NaOH 1M. Bars are the errors of two independent experiments.

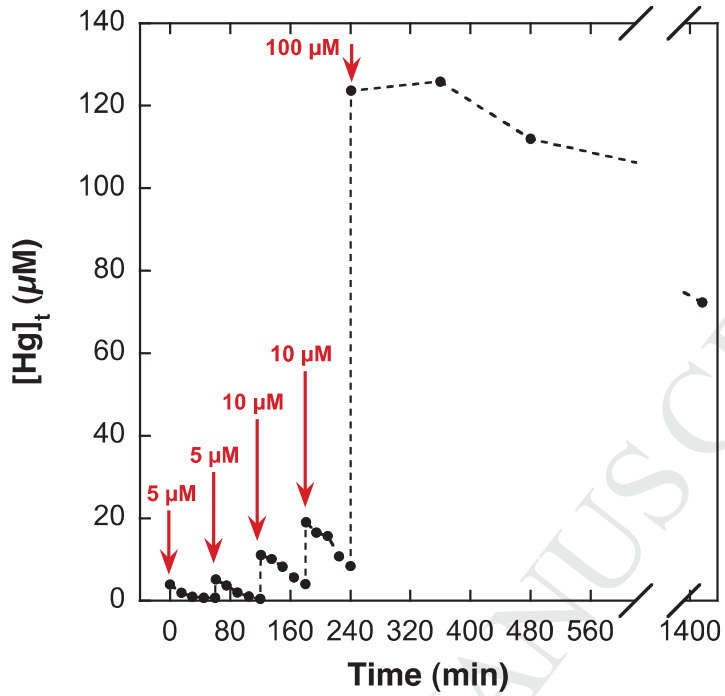

Fig. 6. Kinetics of the Hg^{II} reduction by biologically synthesized hydroxycarbonate green rust ($GR1_{bio}$) with five successive additions of Hg^{II} with an interval of one hour between each addition in the reaction medium containing an initial $GR1_{bio}$ concentration of 400 µM. The quantity of Hg^{II} added each hour is indicated by the value above the red arrow. The total amount of Hg^{II} added in the $GR1_{bio}$ suspension is 130 µM and after 24 h, 77 µM of Hg(II) was reduced into Hg^0.

Highlights bullets

1. The reactivity of green rusts (GR) towards Hg^{II} or methyl red (MR) was tested
2. Bacteria and phosphate did not affect GR reactivity with Hg^{II}
3. Bacteria and ligands (phosphate, silicate and polymers) affect GR reactivity with MR
4. Environmental substances may hinder GR reactivity as regards to the target pollutant

Supplementary information of:

Pseudo-first-order reaction of chemically and biologically formed green rusts with Hg^{II} and $C_{15}H_{15}N_3O_2$: effects of pH and stabilizing agents (phosphate, silicate, polyacrylic acid, and bacterial cells)

P.-Ph. Remy[1, 2], M. Etique[1, 2], A.A. Hazotte[1, 2,§], A.-S. Sergent[1, 2], N. Estrade[3, 4#], C. Cloquet[3, 4], K. Hanna[5, 6], and F.P.A. Jorand[1,2*]

[1]Université de Lorraine, LCPME, UMR 7564, Villers-lès-Nancy, F-54601, France

[2]CNRS, LCPME, UMR 7564, Villers-lès-Nancy, F-54601, France

[3]CNRS, CRPG, UMR 7358, BP 20, Vandœuvre-lès-Nancy, F-54501, France

[4]Université de Lorraine, CRPG, UMR 7358, BP 20, Vandœuvre-lès-Nancy, F-54501, France

[5]ENSCR, CNRS, UMR 6226, CS 50837, Rennes Cedex 7, F-35708, France

[6]Université européenne de Bretagne, Rennes, F-35000, France

[§]Present address: LUNAM University, Subatech-LPGN, UMR 6457 & 6112, BP 92208, F-44322 Nantes Cedex 3, France

#Present address: Pacific Centre for Isotopic and Geochemical Research, EOAS, The University of British Columbia, 2207 Main Mall, Vancouver, British Columbia, V6T 1Z4, Canada.

*Corresponding author: frederic.jorand@univ-lorraine.fr; +33 (0)383 685 248

Table S1: Total mercury concentration in each compound used for experimentation with mercury test.

	Pure water	**$SnCl_2$**	**$GR1_{bio}$**	**$GR1_{ab+P}$**	**$GR2_{ab}$**	***Sp***	**$Fe^{II}_{aq.}$**	**Hg^{II}**	**$GR1_{ab}$**
Hg (ppb)	0.482	0.760	0.370	1.872	0.315	0.574	0.519	104.514	ND

Table S2a : d_{hkl} (nm) parameters from XRD analysis for chemically synthesized and biogenic carbonated green rust from the present study ($GR1_{ab+P}$, $GR1_{ab}$, and $GR1_{bio}$) and from the literature [a](Drissi *et al.*, 1995), [b](Zegeye *et al.*, 2007).

n.d. : no data

Relative intensity	hkl	d_{hkl} $GR1_{ab+P}$	d_{hkl} $GR1_{ab}$	d_{hkl} $GR1_{bio}$	Ref[a] abiotic	Ref[b] biotic
100	003	0.759	0.758	0.759	0.751	0.751
32	006	0.377	0.379	0.378	0.373	0.375
1	101	0.274	-	0.274	0.273	n.d.
15	012	0.268	-	0.268	0.265	0.266
3	104	0.247	-	0.248	0.247	n.d.
12	015	0.235	0.235	0.235	0.233	0.233
1	107	0.209	-	0.209	0.208	n.d.
9	018	0.198	0.197	0.197	0.196	0.196
1	0012	0.189	0.189	0.188	0.188	n.d.
2	1010	0.175	-	0.174	0.173	n.d.

Table S2b : d_{hkl} (nm) parameters from XRD analysis for chemically synthesized hydroxysulfate green rust from the present study ($GR2_{ab}$) and from the literature [a](Simon *et al*., 1997), [b](Hansen *et al*., 1994).

n.d. : no data

Relative intensity	hkl	d_{hkl} $GR2_{ab}$	Ref[a]	Ref[b]
100	001	1.091	1.09	1.10
80	002	0.547	0.545	0.549
60	003	0.365	0.362	0.366
20	004/100	0.276	0.275	0.275
30	101	0.67	0.266	0.226
30	102	0.246	0.245	n.d.
30	005/103	0.220	0.219	0.2195

<u>Table S3</u>. Mössbauer hyperfine parameters of spectra measured at 7, 150 and 12 K for the $GR1_{bio}$, $GR1_{ab+P}$ and $GR2_{ab}$ synthesized according to Zegeye *et al.* (2007), Bocher *et al.* (2004), and Ruby *et al.* (2006), respectively. The $GR1_{bio}$ Mössbauer spectrum indicates the presence of 20 % of a Fe^{II}-Fe^{III} phase assumed to be magnetite in the sample (four sextets). However, no trace of magnetite was detected with XRD under anoxic conditions, and we cannot exclude that the presence of magnetite could be due to an oxidation of $GR1_{bio}$ exposed to ambient air before the Mössbauer analysis. $GR1_{ab}$ was not characterized by TMS, and its ratio Fe^{II}/ Fe^{III} was determined by colorimetry (Ferrozine) on the solid phase.

		□ (0.11 ± 4 mm s^{-1})	Δ *or*□□□ (mm s^{-1})	*H* (kOe)	*RA* *(%)*
	D_1 (Fe^{II}_{GR})	1.25	3.13		22.6%
$GR1_{bio}$	D_2 (Fe^{II}_{GR})	1.24	2.64		26.1%
	D_3 (Fe^{III}_{GR})	0.42	0.51		30.4%
					Fe^{II}/Fe^{III} = 1.6
	S_1 (Fe_3O_4?)	0.69	-0.19	523	
	S_2 (Fe_3O_4?)	0.24	0.25	493	
	S_3 (Fe_3O_4?)	1.72	0.21	383	
	S_4 (Fe_3O_4?)	0.33	0.56	267	
	D_1 (Fe^{II}_{GR})	1.10	2.93		28 %
$GR1_{ab+P}$	D_2 (Fe^{III}_{GR})	0.25	0.36		45 %
	D_3 (Fe^{II}_{GR})	1.10	2.57		27 %
					Fe^{II}/Fe^{III} = 1.2
$GR2_{ab}$	D_1 (Fe^{II}_{GR})	1.31	2.91		66 %
	D_2 (Fe^{III}_{GR})	0.49	0.47		34 %
					Fe^{II}/Fe^{III} = 2.0
$GR1_{ab}$		ND	ND	ND	2.2*

□□(□□□to metallic alpha-iron at room temperature; Δ or 2ε (mm s^{-1}) quadrupole splitting; *H* (kOe) hyperfine field; □□□□□□□□□□□□□□□□□□□□□□□□□□.

*determined by ferrozine measurement

Table S4. Values of pH for batch experiments (n=2) before (initial pH) and after 60 min of incubation (final pH) with Hg^{II}.

Batch experiment	Initial pH	final pH
$SnCl_2$	2.4	2.4
$GR2_{ab}$	7.0 ± 0.2	6.6 ± 0.1
	8.0 ± 0.1	7.2 ± 0.1
	9.5 ± 0.1	8.9 ± 0.3
$GR2_{ab+cells}$	7.0 ± 0.1	6.5 ± 0.1
$GR1_{bio}$	7.0 ± 0.1	7.2 ± 0.3
	8.1	8.0
	9.5 ± 0.1	9.0 ± 0.6
$GR1_{ab}$	8.2 ± 0.1	9.0 ± 0.1
$GR1_{ab+P}$	7.0 ±0.1	7.6 ± 0.3
	8.0 ± 0.1	8.0 ± 0.2
	9.5 ± 0.1	8.8 ± 0.3
Fe^{II} (2mM)	3.3 ± 0.1	3.5 ± 0.1

Note S1. Calculation of structural Fe^{II}

$[Fe^{total}] = [Fe^{II}] + [Fe^{III}] = [GR] \times 6$

$[Fe^{II}]/[Fe^{III}]$ = Mössbauer ratio

e.g. $GR1_{ab+P}$

$[Fe^{II}] = 1.2 \times [Fe^{III}]$

$1.2 \times [Fe^{III}] + [Fe^{III}] = [Fe^{total}]$

$[Fe^{III}] = [Fe^{total}]/2.2$

$[Fe^{II}] = [Fe^{total}] - [Fe^{total}]/2.2 = 1.63$ mM

$[Fe^{II}]GR1_{ab+P} = 1.63\times10^{-3}$ M

$[Fe^{II}]GR1_{bio} = 1.5\times10^{-3}$ M

$[Fe^{II}]GR2_{ab} = 2\times10^{-3}$ M

$[Fe^{II}]GR1_{ab} = 2\times10^{-3}$ M

Note S2. Calculation of k_{FeII} (L mol^{-1} min^{-1}) = k_{obs} normalized to the structural Fe^{II} concentration.

$k_{FeII} = k_{obs} / [Fe^{II}]GR$

Where

$[Fe^{II}]GR$ is the structural Fe^{II} concentration (mol L^{-1})

Note S3. Calculation of k_s (L $mmol^{-1}$ min^{-1}) = k_{obs} normalized to the surface Fe^{II} sites (μM) (see manuscript)

$k_s = k_{obs}$/(surface Fe^{II} sites)

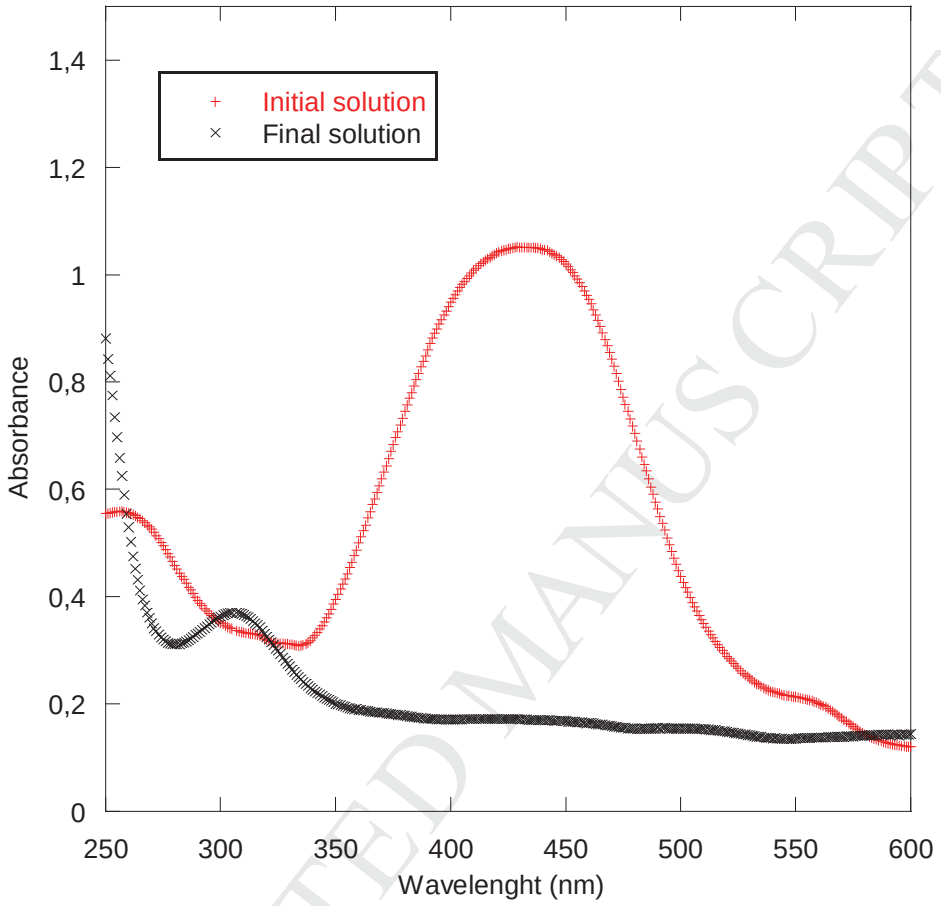

81

82 **Figure S1**: UV-Vis spectra of initial MR solution (+) and the same solution after 300 min of

83 incubation with 500 µM $GR2_{ab}$ (×).

84

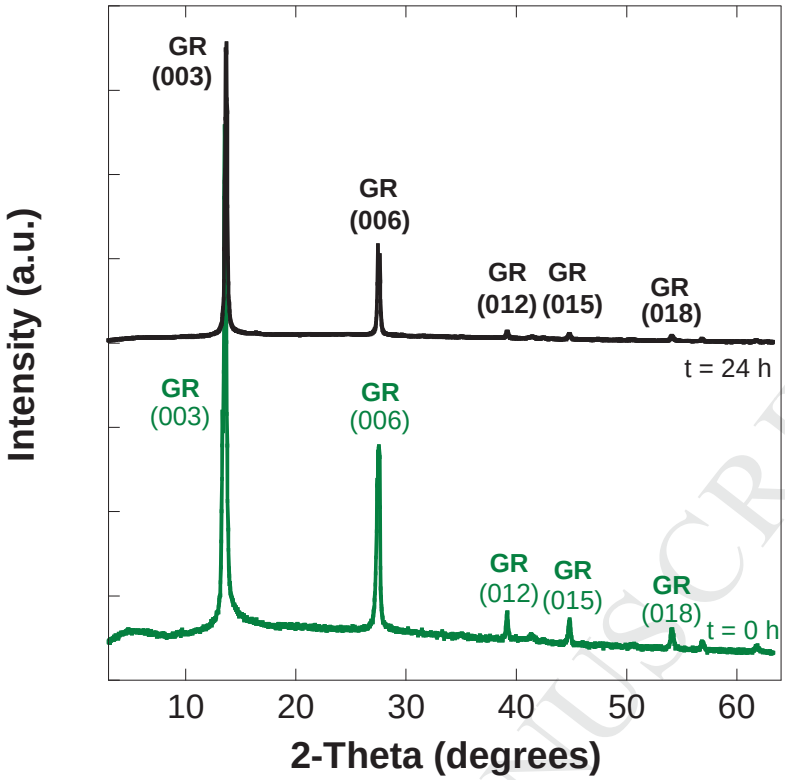

85

86 **Figure S2**. X-ray diffractograms of biologically synthesized hydroxycarbonate green rust
87 ($GR1_{bio}$) before addition of Hg^{II} at the concentration of 5 µM (green line, t = 0 h), and 24 h
88 after (black line, t = 24 h). The initial concentration of $GR1_{bio}$ was 400 µM. The lattice planes
89 of green rust (GR) are written in brackets. The intensity is expressed in arbitrary unit (a. u.).

90

Figure S3: Mössbauer spectra of a) $GR1_{bio}$, b) $GR1_{ab+P}$, and c) $GR2_{ab}$.

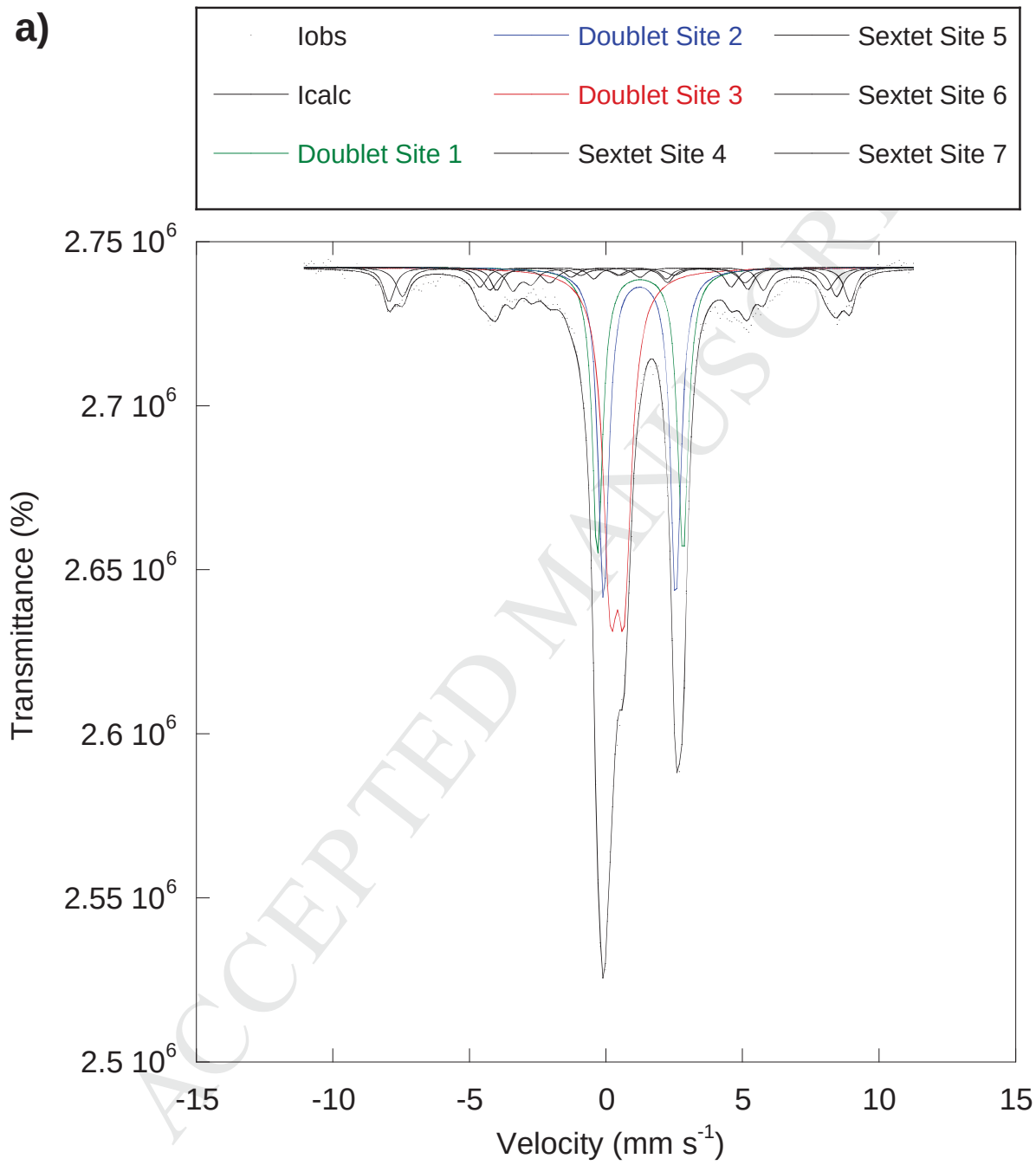

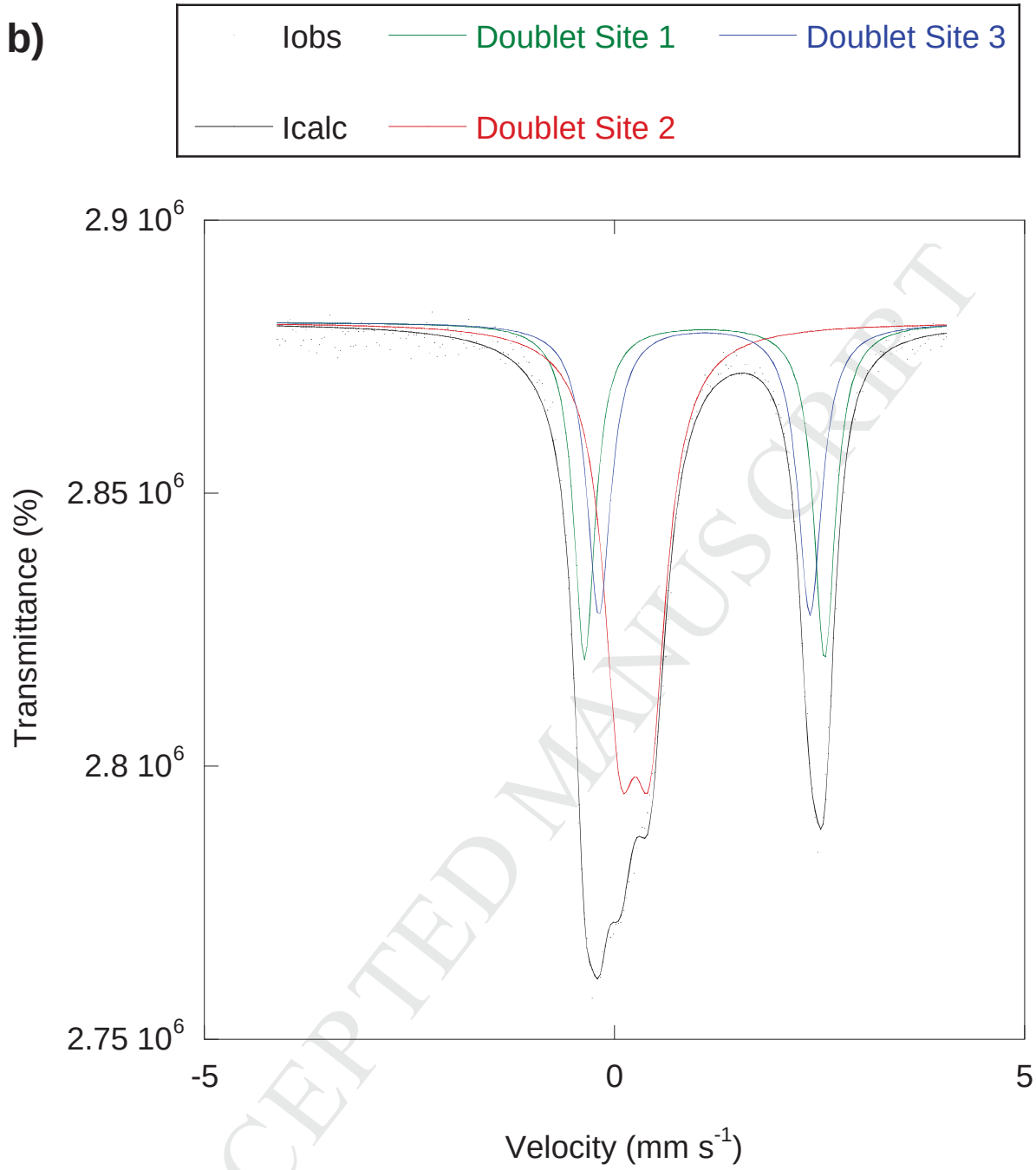

Fig. S3 b) $GR1_{ab+P}$

c)

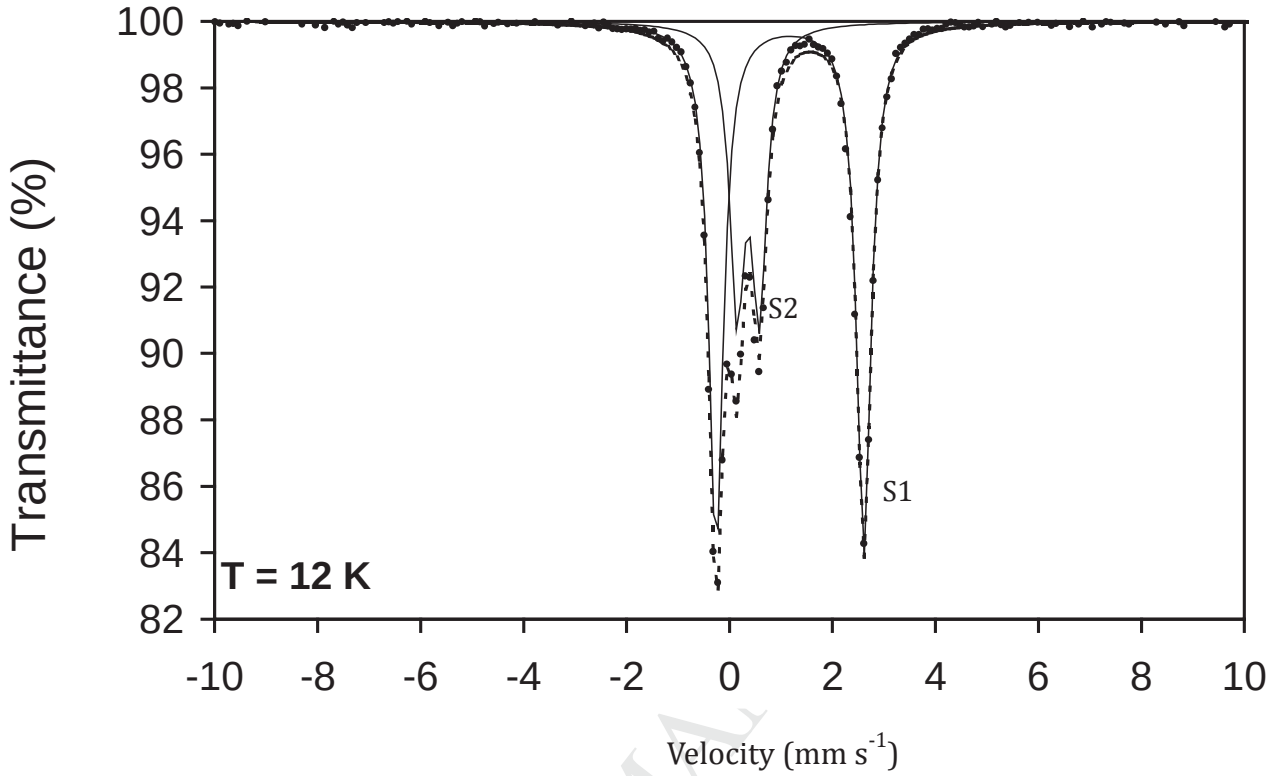

Figure S3c GR2$_{ab}$

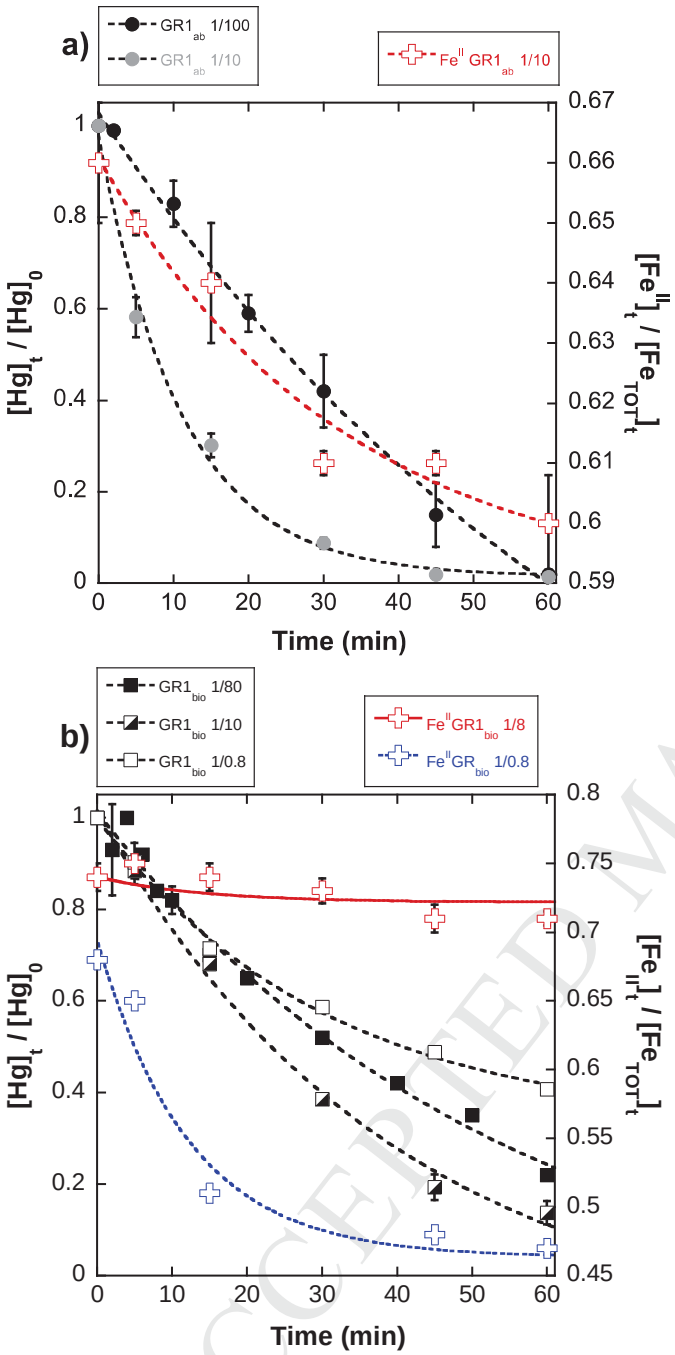

Figure S4. Removal of mercury and oxidation of ferrous iron content of chemically synthesized green rust ($GR1_{ab}$, a) and biologically formed green rust ($GR1_{bio}$, b) over the time at pH 8.2. The initial concentration of Hg^{II} species was 5 µM and the initial concentrations of green rusts used were 4 µM, 40 µM, 400 µM for $GR1_{bio}$, and 50 µM, 500 µM for $GR1_{ab}$. The Hg^{II}/GR ratios were 1/0.8, 1/8, 1/80 and 1/10, 1/100 respectively. Error bars were drawn for two independent assays.

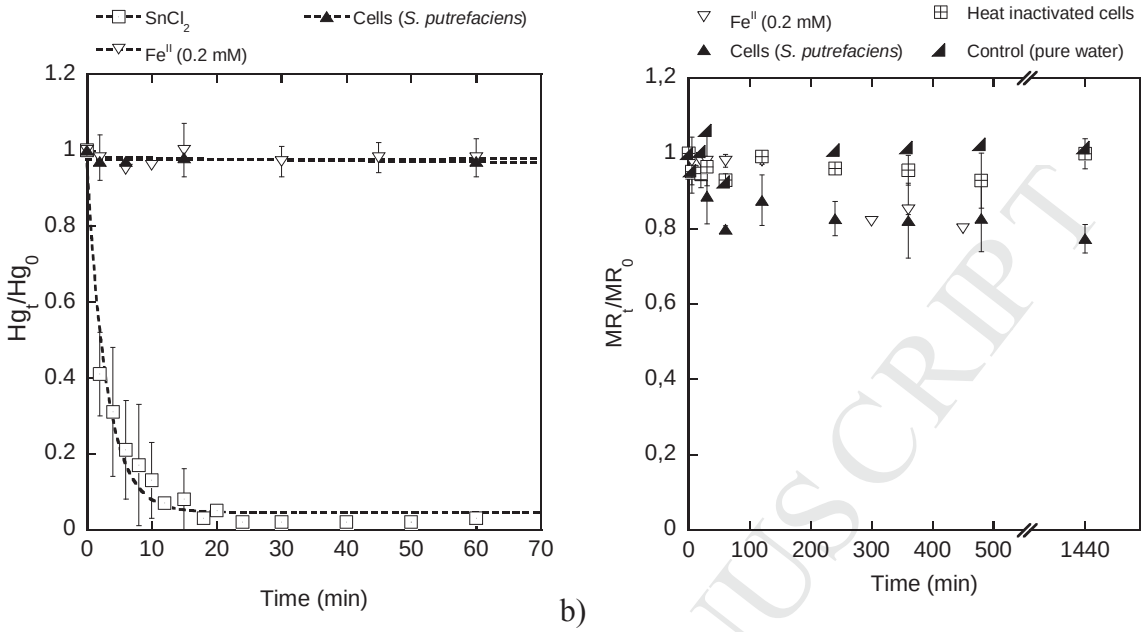

a) b)

Figure S5. (a): Disappearance of mercury over time in the presence of 50 µM Sn^{II} (pH 3.0 ± 0.5), and 0.2 mM aqueous Fe^{II} (pH 7.0 ± 0.1) or 6×10^5 cells mL^{-1} of *Shewanella putrefaciens* (pH 7.0 ± 0.1) (cells), a cell density that is equivalent to that used for the synthesis of GR_{bio} and that is expected to remain with $GR1_{bio}$. The changes in pH after a 60 h incubation time period are reported in Table S7. Bars are the errors of two independent experiments. The stannic solution ($SnCl_2$, 50 µM pH = 3) was prepared from a stock solution (22.5 mM in HCl 1.5 M) ($SnCl_2$ salt, 98% anhydrous, 196981000, Acros). It was used as an indicator for Hg^{II} reduction, since Sn^{II} is known to be a powerful reducer (Zheng and Hintelmann, 2010). In order to avoid Sn^{II} precipitation, which can occur along with increasing pH, Hg^{II} reduction by aqueous Sn^{II} were only performed at pH 3.

(b): Disappearance of methyl red (MR) over time in the presence of 0.2 mM aqueous Fe^{II} (pH 7.0), 6×10^5 cells mL^{-1} of a fresh *S. putrefaciens* suspension (cells) or heat inactivated cells (dead Sp cells), or a solution of MR in pure water.

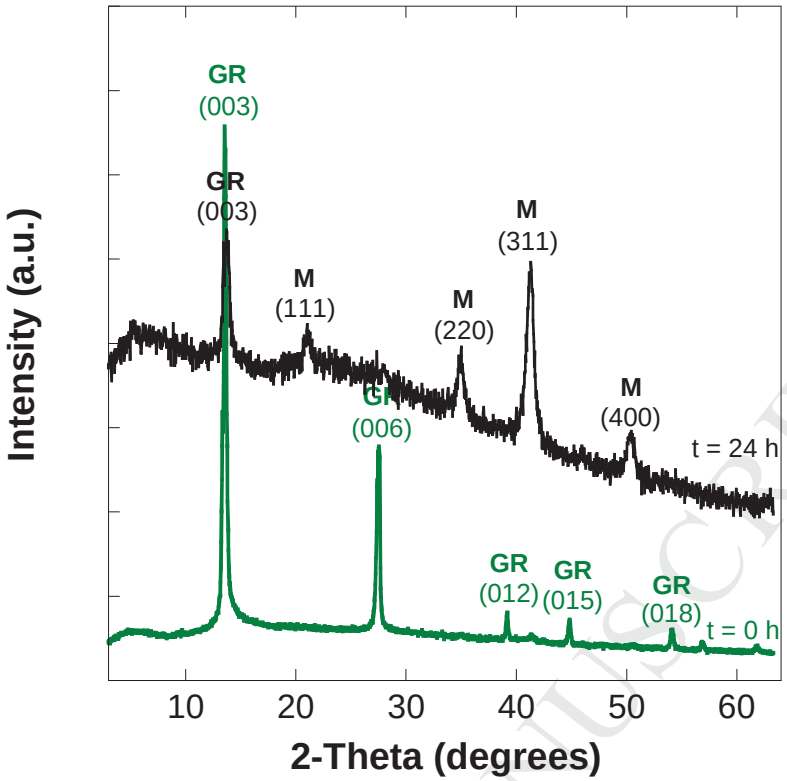

128

129 **Figure S6**. X-ray diffractograms of biologically synthesized hydroxycarbonate green rust
130 ($GR1_{bio}$) before addition of Hg^{II} at the concentration of 5 µM (green line, t = 0 h), and 24 h
131 after (black line, t = 24 h). The initial concentration of $GR1_{bio}$ was 4 µM. The green rust (GR)
132 was oxidized into magnetite (M) during the reduction of mercury. The lattice planes are
133 written in brackets. The intensity is expressed in arbitrary unit (a. u.).

134

135

136 References for supplementary data:

137 Bocher, F., Géhin, A., Ruby, C., Ghanbaja, J., Abdelmoula, M., Génin J-M.R. 2004.
138 Coprecipitation of Fe(II–III) hydroxycarbonate green rust stabilized by phosphate
139 adsorption. Solid State Sciences, 6 (1), 117–124.
140 Drissi, SH, Refait, P, Abdelmoula, M, Génin, J.-M.R. 1995. The preparation and
141 thermodynamic properties of iron(II)-iron(III) hydroxide-carbonate (green rust); Pourbaix
142 diagram of iron in carbonate-containing aqueous media. Corrosion Science 37, 2025–
143 2041.
144 Hansen H. C. B., Borgaard O. K., Sorensen J. 1994. Evaluation of the free energy of
145 formation of Fe(II)-Fe(III) hydroxide-sulphate (green rust) and its reduction of nitrite.
146 Geochimica et Cosmochimica Acta 58, 2599-2068.
147 Ruby, C., Haissa, R., Géhin, A., Abdelmoula, M., Génin, J.-M.R., 2006. Chemical stability of
148 hydroxysulphate green rust synthesized in the presence of foreign anions: carbonate,
149 phosphate and silicate. Hyperfine Interactions, 167: 803-807.
150 Simon L., Francois M., Refait P., Renaudin G., Lelaurain M., and Génin J.-M. R., 2003.
151 Structure of the Fe(II-III) layered double hydroxysulphate green rust two from Rietveld
152 analysis. Solid State Sciences 5, 327–334.
153 Zegeye, A., Ruby, C., Jorand, F., 2007. Kinetic and thermodynamic analysis during
154 dissimilatory γ-FeOOH reduction: formation of green rust 1 and magnetite.
155 Geomicrobiology Journal 24, 51-64.
156 Zheng, W., Hintelmann, H., 2010. Nuclear field shift effect in isotope fractionation of
157 mercury during abiotic reduction in the absence of light. The Journal of Physical
158 Chemistry A 114 (12), 4238-4245.